JGR Planets

RESEARCH ARTICLE

10.1029/2023JE007859

Magnetospheric-Ionospheric-Atmospheric Implications From the Juno Flyby of Ganymede

J. H. Waite Jr.[1], T. K. Greathouse[2], S. R. Carberry Mogan[3], A. H. Sulaiman[4], P. Valek[2], F. Allegrini[2], R. W. Ebert[2], G. R. Gladstone[2], W. S. Kurth[5], J. E. P. Connerney[6], G. Clark[7], F. Bagenal[8], S. Duling[9], N. Romanelli[10,11], S. Bolton[2], A. Vorburger[12], C. Paranicas[7], P. Kollmann[7], B. Mauk[7], C. Hansen[13], D. Buccino[14], R. E. Johnson[15], R. J. Wilson[8], and B. Teolis[2]

[1]Waite Science LLC, Pensacola, FL, USA, [2]Division of Space Science and Engineering, Southwest Research Institute, San Antonio, TX, USA, [3]Space Sciences Laboratory, University of California Berkeley, Berkeley, CA, USA, [4]School of Physics and Astronomy, Minnesota Institute for Astrophysics, University of Minnesota, Minneapolis, MN, USA, [5]Physics and Astronomy, University of Iowa, Iowa City, IA, USA, [6]Space Research Corporation, Annapolis, MD, USA, [7]Johns Hopkins, Applied Physics Laboratory, Laurel, MD, USA, [8]Laboratory for Atmospheric and Space Physics, University of Colorado, Boulder, CO, USA, [9]University of Cologne, Institute for Geophysics and Meteorology, Cologne, Germany, [10]Department of Astronomy, University of Maryland, College Park, MD, USA, [11]NASA Goddard Space Flight Center, Greenbelt, MD, USA, [12]Physics Institute, University of Bern, Bern, Switzerland, [13]Planetary Science Institute, Tucson, AZ, USA, [14]Jet Propulsion Laboratory, NASA, Pasadena, CA, USA, [15]University of Virginia, Charlottesville, VA, USA

Abstract Juno flew over the northern mid-latitudes of Ganymede during orbit 34 of the Juno mission, reaching an altitude of 1,053 km (16:56:07.972 UTC) at a sub spacecraft latitude/longitude of 33.66N, 57.5W degrees on 7 June 2021. Between 16:43 and 17:02 UT, Juno pierced Ganymede's magnetosphere at a velocity relative to Ganymede of 18.57 km s^{-1}. Juno's instrumentation provided a unique opportunity to sample the local environment of Ganymede and its magnetosphere. We present measurements of the composition of the polar ionospheric outflow and the energetic electrons that penetrate Ganymede's atmosphere and produce its aurora. When these new observations are combined with modeling, conclusions can be drawn that affect our understanding of the atmosphere of Ganymede. The measured JADE precipitating plasma electrons provide an energy flux beyond that needed to create the observed oxygen emissions measured by UVS, but the electron energy spectrum is optically thin to the sparse atmosphere and does not provide the observed oxygen ultraviolet emission unless the O_2 column density is increased by over an order of magnitude compared to previous atmospheric models. More than 99% of the electron energy flux passes through the atmosphere into the ice, thereby increasing the H_2 and O_2 content of the atmosphere. The increased H_2 and O_2 production is largely responsible for increasing the oxygen column density to a level that produces within known uncertainties the OI135.6 and OI130.4 nm emissions when bombarded by the electron energy flux observed by JADE. This suggests that past modeling efforts have underestimated the density of the atmosphere by over an order of magnitude.

Plain Language Summary Juno flew by the Jovian satellite Ganymede on orbit 34 of the mission coming within 1,053 km of the surface at high northern latitudes. Juno provides a unique data set from the particle, field, and ultraviolet imaging experiments that can be utilized to study the interaction between the magnetosphere of Ganymede and the magnetosphere of Jupiter. Compositionally diverse ion outflow was observed in the northern polar cap that can be linked to the exchange of plasma and energetic particles between Jupiter and Ganymede. Furthermore, an electron spectrum produced by magnetic reconnection processes was observed that can be linked to the aurora at Ganymede. These observations provide new information about Ganymede's atmosphere. They strongly suggest an increase in the column density of O_2 in Ganymede's atmosphere of an order of magnitude relative to all previous models. The latter has implications for all water ice satellites in the outer solar system.

Key Points:

- Multiple data sets from Juno's flyby of Ganymede indicate energetic particle impact of the surface and atmosphere resulting in ion outflow
- Reconnection processes on the Jupiter-facing flank of the magnetospheric interaction provide constraints on the auroral excitation
- Initial modeling strongly suggests an order of magnitude increase in atmospheric O_2 column density relative to previous models

Correspondence to:

J. H. Waite,
hunterwaite@gmail.com

Citation:

Waite, J. H., Jr., Greathouse, T. K., Carberry Mogan, S. R., Sulaiman, A. H., Valek, P., Allegrini, F., et al. (2024). Magnetospheric-ionospheric-atmospheric implications from the Juno flyby of Ganymede. *Journal of Geophysical Research: Planets*, *129*, e2023JE007859. https://doi.org/10.1029/2023JE007859

Received 19 APR 2023
Accepted 16 FEB 2024

Author Contributions:

Conceptualization: J. H. Waite, A. H. Sulaiman, F. Bagenal, S. Bolton, B. Mauk, C. Hansen
Formal analysis: J. H. Waite, S. R. Carberry Mogan, P. Valek, F. Allegrini, R. W. Ebert, W. S. Kurth, J. E. P. Connerney, S. Duling, N. Romanelli, A. Vorburger, C. Paranicas, D. Buccino
Funding acquisition: J. E. P. Connerney, S. Bolton
Investigation: J. H. Waite, T. K. Greathouse, P. Valek, F. Allegrini, R. W. Ebert, G. Clark, P. Kollmann, R. E. Johnson, B. Teolis
Methodology: J. H. Waite, R. W. Ebert, S. Bolton, B. Mauk, R. E. Johnson
Project administration: J. E. P. Connerney, S. Bolton, C. Hansen

1. Introduction

Ganymede is the largest moon in the solar system and the only known moon in the solar system with an intrinsic magnetic field (Ansher et al., 2017; Gurnett et al., 1996; Kivelson et al., 1996; Weber et al., 2022; Williams et al., 1998). Jupiter has a rotation period of 9 hr55 m29.7 s and its planetary magnetic dipole is tilted ~10 deg

Resources: J. H. Waite
Supervision: J. H. Waite, J. E. P. Connerney, F. Bagenal, B. Mauk, C. Hansen
Visualization: J. H. Waite, T. K. Greathouse, S. R. Carberry Mogan, A. H. Sulaiman, G. R. Gladstone, G. Clark, S. Duling, N. Romanelli, A. Vorburger, D. Buccino
Writing – original draft: J. H. Waite
Writing – review & editing: J. H. Waite, T. K. Greathouse, S. R. Carberry Mogan, P. Valek, F. Allegrini, R. W. Ebert, G. R. Gladstone, W. S. Kurth, G. Clark, F. Bagenal, N. Romanelli, S. Bolton, A. Vorburger, C. Paranicas, P. Kollmann, C. Hansen, D. Buccino, R. E. Johnson, R. J. Wilson, B. Teolis

(Connerney et al., 2022) from the planetary rotation axis. Ganymede is in a phase locked orbit around Jupiter with a period of about 7 days at a distance from Jupiter of 14.97 R_J ($1R_J$ = Jovian radius = 71,492 km; 1 R_G = Ganymede radius = 2634.1 km). Ganymede was at 21:00 to 22:00 hr solar local time in its orbit about Jupiter when the Juno encounter occurred on 7 June 2021.

A large fraction of the plasma residing in Jupiter's equatorial magnetospheric disk can be traced back to Io and Europa. These ions are confined around a "centrifugal equator" that is located between the spin equator and the magnetic equator, so the flux of particles onto Ganymede varies in time. Given that the Alfvénic Mach number is <1, magnetic pressure plays a predominant role in confining Ganymede's magnetosphere. This produces a sub-Alfvénic, subsonic, and time dependent interaction between Ganymede's magnetic field and the pressure produced by Jupiter's approximately corotating flow of plasma and energetic particles present in Jupiter's equatorial magnetosphere. The offset of the rotation axis of Jupiter from the magnetic dipole axis results in a cyclical traversal of Jupiter's centrifugally confined plasma disk that varies with the synodic period of the orbital motion of Ganymede about Jupiter. Ganymede was near the center of Jupiter's plasma disk during the Juno encounter, which maximizes the plasma and energetic particle pressure of the Jupiter-Ganymede magnetospheric interaction during the encounter. Since Ganymede's orbital velocity about Jupiter is 10.88 km s^{-1} and Jupiter's interacting plasma rotates at a speed ∼150 km s^{-1}, the plasma disk overtakes Ganymede in its orbit, initiating an interaction over the trailing hemisphere of its Keplerian orbit about Jupiter. The Juno spacecraft entered the magnetospheric domain of Ganymede in the downstream tail interaction region of the corotating plasma with a view of the nightside of Ganymede and exited in the direction of the sub-Jovian upstream interaction region (see Figure 1), which was on the solar illuminated hemisphere of Ganymede.

The Galileo spacecraft made both remote sensing and in situ observations of Ganymede in flyby encounters G1, G2, G7, G8, G28, and G29 between 1995 and 2003. Flybys G1 and G2 were of particular interest in identifying the intrinsic magnetic field of Ganymede and determining the basic characteristics of its ionosphere (Jia et al., 2008). All the Galileo flybys have been utilized (Duling et al., 2014; Jia et al., 2008) to model its magnetospheric interaction. Hubble Space Telescope (HST) observations provided an additional remote sensing perspective on the magnetospheric interaction by measuring Ganymede's aurora (Feldman et al., 2000; McGrath et al., 2013) and suggesting that the auroral structure seen at mid-latitudes near the surface represents the boundary between closed magnetic fields with both feet on Ganymede's surface and open magnetic field lines with one foot on Ganymede and the other attached to Jupiter. HST also provided valuable information about the composition and density of Ganymede's atmosphere through the measurement of ultraviolet emissions from O_2 and H_2O (Hall et al., 1998; Roth et al., 2021).

The modern instrumentation onboard Juno allows a new level of quantification of the magnetospheric processes operating in the Ganymede-Jupiter interaction system (Bagenal et al., 2017; Bolton et al., 2017; Connerney et al., 2017; Gladstone et al., 2017; Hansen et al., 2022; Kurth et al., 2017; Mauk et al., 2017; McComas et al., 2017). Of noteworthy relevance during the flyby are the clear identification of changing particle and field characteristics that take place in discrete boundaries during the close flyby (Allegrini, Bagenal, et al., 2022; Clark et al., 2022; Kurth et al., 2022), ionospheric outflows of H^+, H_2^+, H_3^+, O_2^+, and O^+ with a small admixture of water group ions (Valek et al., 2022a) produced by electron bombardment of the exospheric material, and reconnection processes at the sub Jovian, leading hemisphere magnetospheric boundary that energize electrons (Ebert et al., 2022; Romanelli et al., 2022) and may represent electron populations very similar to those that produce the Ganymede aurora. These measured energetic electrons in the region of the polar cap or at the reconnection site can ionize and excite neutrals and will produce the dissociative excitation of O_2 that is identified with the aurora. The ions that are produced through ionization of the atmosphere are subject to the electromagnetic fields near Ganymede. Such superthermal ion populations would not be detected by Juno at the altitudes of the measurements and could play a role in sputtering the atmosphere in the auroral zone region in a manner suggested for O^+ by Leblanc et al. (2017).

In what follows the 2.0 Observation section presents the relevant fields, particles, ultraviolet spectral imaging, and radio occultation observations obtained during the Juno flyby. Section 3 provides new modeling and analysis concerning: (a) the high latitude magnetic field structure and (b) modeling and analysis that use the new observations to improve our understanding of the atmosphere and ionosphere. Finally, we provide a Summary in Section 4.

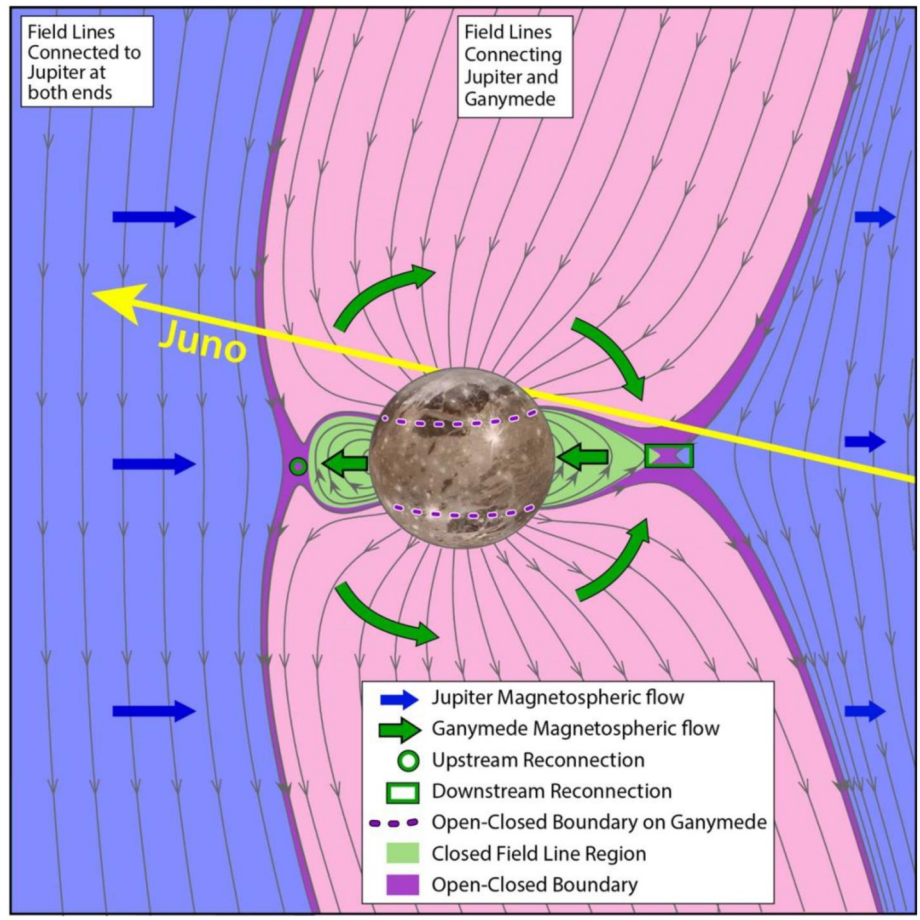

Figure 1. Artist rendering of the flyby from a magnetospheric interaction point of view. Note; 1) the position in solar local time of Ganymede in its orbit about Jupiter is 22 hr. 2) The angular offset of the plasma disk with respect to the orbital plane is ~10° and Ganymede's relative position in the plasma disk during the flyby is approximately 1.8° south of the center at the time of encounter. The figure illustrates the plasma and magnetic field directions near Ganymede relative to the Juno spacecraft trajectory. The yellow arrow of Juno's motion has a component in the plasma flow direction (which is all we illustrate here). But note by examining the 3D trajectory in Figure 2, Juno is also moving toward Jupiter during the encounter.

2. Observations

Particle and field observations were used in conjunction with ultraviolet spectral images, and radio occultation profiles of the ionosphere to perform the analysis reported in this paper.

2.1. Overview of the PJ34 Flyby Magnetospheric Interaction Data Set

Boundary crossings reflected in the fields and particle signatures with the aid of modeling help us to better understand the processes at play in the Ganymede-Jupiter interaction regions of interest. The first boundary encountered was at 16:43 UT (see Figure 2, MIP A). The magnetometer (MAG) observed a change in the magnetic field orientation and a decrease in field magnitude (Connerney, John, 2017; Romanelli et al., 2022). The Juno Auroral Distribution Experiment (JADE) reported an increase in the heavy ion flux (i.e., the plasma energy range) as the spacecraft entered the downstream or "Wake" region of the magnetospheric interaction with Jupiter (Allegrini, Bagenal, et al., 2022; Allegrini, Wilson, Ebert, & Loeffler, 2022). Bursty plasma wave emissions measured by Waves began within the Ganymede magnetospheric wake (Kurth et al., 2022). The energetic electron fluxes measured by the Juno Energetic Particle Detector Instrument (JEDI) were reduced in flux relative to the surrounding Jovian magnetospheric medium pre- and post-encounter at almost all JEDI energies during the time that Juno traversed Ganymede's wake and when Juno was on polar field lines (Clark et al., 2022; Li et al., 2022; Mauk, 2022) as a result of energetic particles lost to Ganymede during the magnetospheric interaction process.

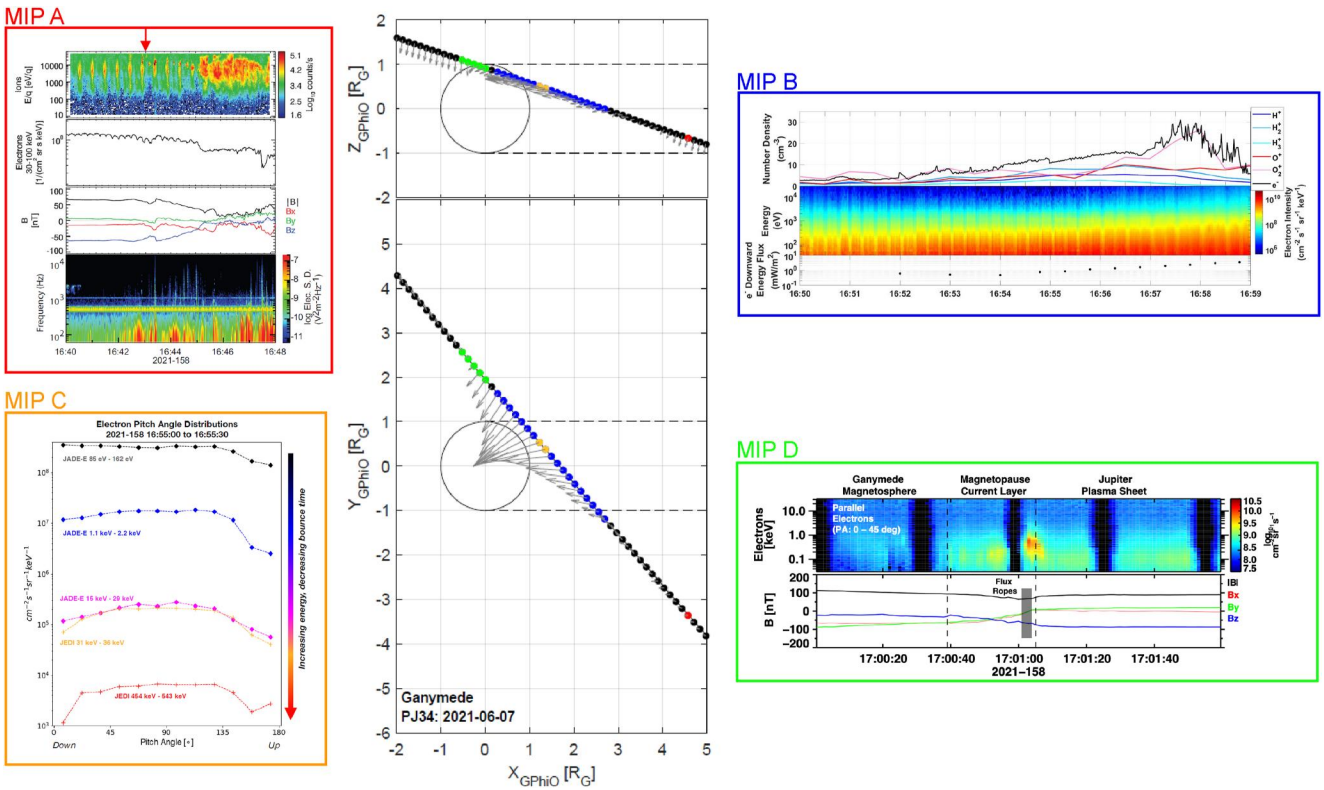

Figure 2. The central portion of the figure shows an orbital projection of the flyby trajectory in a GPhiO frame: GphiO is defined here as Ganymede centered with the $+Z$ axis being parallel with Jupiter's spin axis, $+X$ is along the "plasma corotation" direction at Ganymede (parallel to the cross product of $+Z$ with the Jupiter-to-Ganymede vector), and $+Y$ completes the right-handed set (approximately pointing toward Jupiter's center). Multi-Instrument Panel (MIP) A—This first MIP illustrates the boundary crossing at 16:43 UTC. The data sets that comprise the panels are from top to bottom: (a) a JADE ion spectrogram, (b) a JEDI electron spectrum, (c) the vector magnetic field, and (d) a log scale plasma wave spectrogram. Note that the time of the red arrow in the MIP A panel is indicated as a single red point on the trajectory panel of the figure, indicating the time of the discrete boundary crossing event at 16:43 UTC. MIP B is for the region from 16:50 to 16:59 UTC. The instrument panel elements are the JADE ionospheric ion composition, the Upper Hybrid derived electron densities showing the change in character from smooth to spikey (associated with signatures of ion acceleration in the JADE ionospheric ions) at 16:57 UTC, and in the lowest panel the JADE electron energy spectra with a line plot along the bottom showing the change in downward electron energy flux every 30 seconds. MIP C contains data from JADE and from JEDI showing the pitch angle spectra that strongly suggests that Juno was on open magnetic field lines—one end connected to Ganymede's polar cap and the other to Jupiter's ionosphere. MIP D covering 17:00 to 17:02 UTC illustrates the outbound crossing with data from JADE showing the downward electron energy spectrum and MAG data showing the magnetic field rotation and flux rope formation in this region of the interaction.

The most striking bounded region begins at 16:50 UTC with its closure around 17:01 UTC (see Figure 2, MIP B). The appearance of a colder plasma component that is attributed to Ganymede's ionosphere is measured as Juno crosses this magnetopause boundary (Allegrini, Bagenal, et al., 2022). The Waves experiment infers the ionospheric electron densities using upper hybrid emissions (Kurth & Piker, 2022a, 2022b; Kurth et al., 2022) that vary with distance from Ganymede and change in structural character as the spacecraft approaches the outbound magnetopause crossing. The JADE Time of Flight (TOF) ion mass spectrometer identifies outflowing ions from the local ionosphere as determined by their low energy and composition: H^+, H_2^+, H_3^+, O_2^+, O^+ plus unresolved water group ions (Allegrini, Wilson, Ebert, & Loeffler, 2022; Valek et al., 2022a).

A moderate intensity plasma electron population is identified extending from thermal to keV energies with a downward electron component carrying an energy flux of 0.5–1 mW m^{-2}. This downward flux of electrons provides a more than sufficient source of ionization to create the observed ion outflow from the local sputtered atmosphere, which is composed of O_2, H_2, and H_2O. Modeling carried out as part of our analysis suggests that the atmosphere is optically thin to the incoming plasma electrons in the energy range from 35 to 29,000 eV and therefore less than 1% of the incoming electron energy measured by the JADE instrument is absorbed by the local atmosphere, with the remainder striking the surface and, through radiolysis, liberating additional H_2 and O_2. The thin atmosphere under these conditions produces very little observable ultraviolet

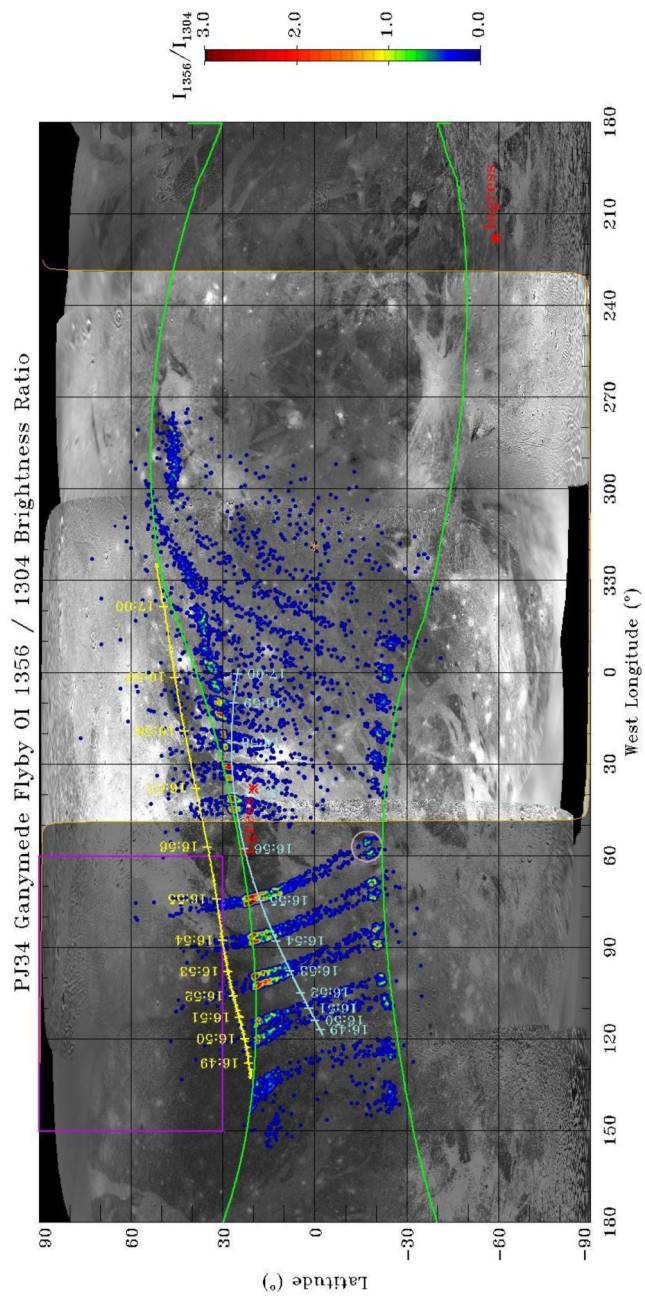

Figure 3. Brightness ratio map (with color bar on right) of Ganymede's atomic oxygen 130.4 and 135.6 nm emissions observed by Juno-UVS (Greathouse et al., 2022) on 7 June 2021, overlaid on a USGS map of Ganymede. https://astrogeology.usgs.gov/search/map/Ganymede/Voyager-Galileo/Ganymede_Voyager_GalileoSSI_global_mosaic_1km. The 130.4/135.6 nm brightness ratio of the better-observed northern aurora decreases at locations nearer to the sub-solar point (orange asterisk). This decrease is expected for a global O_2 atmosphere that becomes dominated by sublimated H_2O in the sub-solar region (Roth et al., 2021). The poleward edge of the auroral emissions is expected to be in close proximity to the last closed field lines of Ganymede's magnetosphere, and MHD models based on flyby conditions (Duling et al., 2022) (green lines) predict auroras in good agreement with the Juno-UVS observations, at least in the downstream hemisphere. The sub-spacecraft (aqua line) and MHD model (Duling et al., 2022) magnetic (yellow lines) footprints of Juno during the flyby are shown, with 1-min tick marks labeled by the UTC time (hh:mm). The ingress and egress ionospheric occultation locations are noted with red symbols at the position of their minimum ray path (Buccino et al., 2022). Note that the average subsolar coordinates over the UVS interval 16:50:39 to 17:04:39 are: latitude = 0.06°, longitude = 318.74°. The deep purple box in the northern open field line region indicates the box over which the emission data was averaged to produce a comparison with the emission model described in the paper. Likewise, the light purple circle shows the location of the auroral vertical profile that was used in comparison with the auroral emission model analysis and is the region that contains the observations displayed in Figure 4.

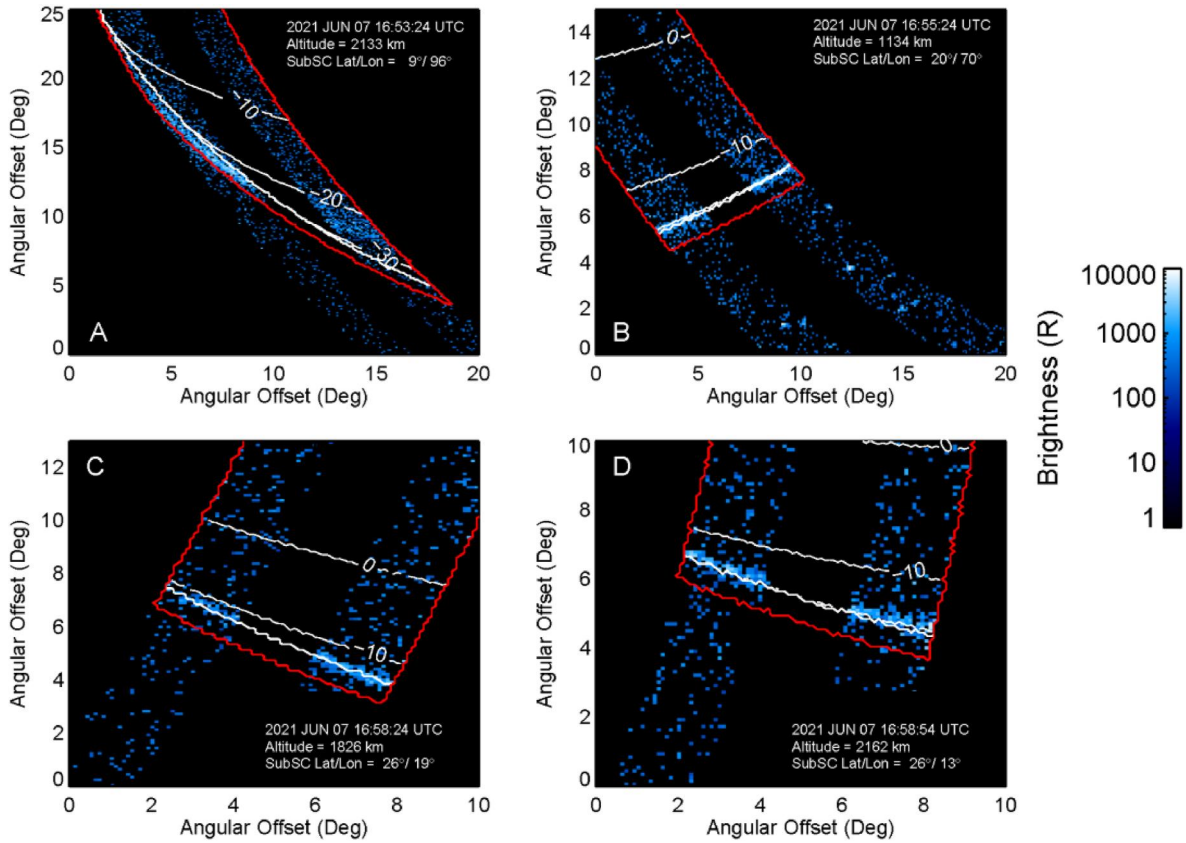

Figure 4. Similar to Figure 2 from Greathouse et al. (2022), this figure shows the mapping of the auroral emissions relative to Ganymede's limb using only a −17 ms shift in time instead of the −34 ms shift originally used. The white contours show latitudes on Ganymede with the thick bottom most nearly horizontal line of the limb. The red contour shows the 50 km altitude mapping. Only the wide slit emissions are shown for clarity (no data from narrow-wide slit, see (Greathouse et al., 2022) for further details).

emissions, consistent with the lack of emission in the high latitude regions noted by the UVS experiment onboard Juno (Greathouse et al., 2022; Trantham, 2014a, 2014b).

A change in the derived electron density is seen by the Waves investigation at 16:57 UTC, where the derived electron density increases and becomes "spiky" in nature (Kurth et al., 2022). At the same time, the JADE TOF sees a pronounced increase in the outflow of O_2^+ as Juno approaches the dayside "leading" magnetopause boundary. These ion flows are reminiscent of the O_2^+ ion outflows modeled by Carnelli et al. (2020a, 2020b) at the flanks of the magnetospheric interaction region. Throughout the time from 16:50 to 17:00 UTC, the pitch angle measurements of the plasma (JADE, Allergini et al., 2022a) and the energetic particles (JEDI, Clark et al., 2022) indicate that the local magnetic field is linked from the polar ionosphere of Ganymede to the Jovian ionosphere by means of an Alfvenic wing structure. There is no evidence in the particle data during Juno's polar traversal of a transition to closed magnetic field lines where both ends of Ganymede's intrinsic magnetic field are tied to Ganymede, which would be observed through low particle intensities at all energies at both small and large pitch angles (see Figure 2, MIP C).

The outbound, upstream sub-Jovian magnetopause boundary crossing between 17:00:39 and 17:01:05 UTC is seen as a region of increased plasma electron flux with a downward component that increases by a factor of ∼10–20 (9 mW m^{-2}) from that in the polar cap (0.5–1.7 mW m^{-2}). The increases in accelerated, streaming electrons are reported to be associated with local magnetic field reconnection processes observed in both the plasma (Ebert et al., 2022) and magnetic field. Magnetic flux ropes are seen in the magnetic field data (Romanelli et al., 2022) (see Figure 2, MIP D). These "reconnection associated" downward electron fluxes are likely representative of the electrons producing the aurora and at 9 mW m^{-2} energy flux have sufficient energy flux to produce the emissions. However, the magnetic field modeling (Duling et al., 2022) does not

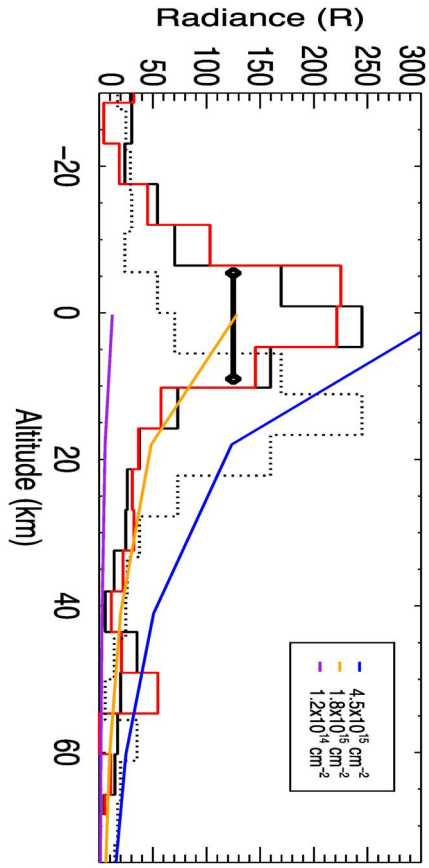

Figure 5. This figure shows the −17 ms shifted auroral emissions versus altitude from either side of the wide slit (black and red solid lines) using data from the spin shown in Figure 4b. The emission amplitude agreement between the two extracted emission rate profiles is an indication of the S/N of the observation. The black dotted line has the same distribution as the black solid line, but with the −34 ms shift applied in Greathouse et al. (2022). The heavy black bar with diamonds on the ends shows the full width half maximum of the Juno UVS spatial resolution on a point source, which suggests that the emission must be localized to a surface boundary layer. The purple, yellow, and blue line traces represent the model results using an auroral electron energy input from the JADE electron spectrometer taken near the open closed magnetic field line boundary. The various colors show the emissions expected for column densities of O_2 from 1.2×10^{14} to 4.5×10^{15} cm^{-2}.

directly link the observed reconnection region with the presumed open/closed magnetic field boundary that UVS identifies as the polar edge of auroral emissions (Greathouse et al., 2022) (see Figure 3).

2.2. UVS Auroral Observations

Initial mapping of the ultraviolet auroral emissions, relative to Ganymede, measured just prior to PJ 34 using the reconstructed kernels archived with NAIF resulted in a strange kink in the otherwise smoothly varying (over latitude and longitude) southern auroral emissions. This issue was pointed out and described in Greathouse et al. (2022). A time shift of −34 msec (to the Stellar Reference Unit, SRU, acquisition time) was required by the SRU imaging of Ganymede to align the SRU image correctly with the USGS base map (Becker et al., 2022). The SRU team believes their time shift to be good at ±5 ms.

Mapping of the Juno UVS observations of Ganymede's auroral emissions was also shown to be improved by a similar shift (−35 ms, Greathouse et al., 2022). Any further attempts at possibly adjusting the time shift more accurately were not attempted as the agreement between the two data sets was taken as confirmation and because the issue of the southern auroral kink was corrected for UVS. However, in our attempt to characterize the particle precipitation and resultant oxygen excitation and emission process, we were forced to take a more precise look at the emissions observed just off the limb of Ganymede. The UVS images of the auroral emission just off Ganymede's surface (Figure 2 of Greathouse et al. (2022)) were made at 0.1° resolution on the sky. These images showed auroral emissions that have a narrow vertical extent and peak at altitudes ∼10–15 km above Ganymede's surface. However, modeling within this paper shows that for a wide variety of atmospheric models of Ganymede, all the auroral emissions are expected to peak at the surface and become fainter with increasing altitude. This is contrary to the UVS observations as mapped. When a slightly reduced shift of −17 ms rather than −35 ms is applied to the UVS data set, this seems to correct the kink in the southern aurora discussed in Greathouse et al. (2022) as well as places the observed limb emissions near Ganymede's surface (Figures 4 and 5).

There are three issues of note concerning the uncertainties of the mapping for UVS, besides the obvious fact that UVS does not actually detect the limb of Ganymede directly. The first is that while the nominal spatial resolution of an object observed through Juno UVS' wide slits is 0.2° on the sky, when the scan mirror is rotated to adjust the FOV of Juno UVS, it imparts a tilt of the slit with respect to the spin axis of the spacecraft. This tilt reduces the spatial resolution on the sky by a factor of $1/[\cos(\theta)]^2$ (Greathouse et al., 2013), where θ is the angle of the scan mirror away from the spin plane. As Juno approached Ganymede UVS, the scan mirror was set to position 81 ($\theta = 27.06°$); then, after the FOV crossed Ganymede's disk, we repositioned the scan mirror to position 0 ($\theta = -30.21°$) to capture Ganymede as we flew away. The scan mirror angles versus mirror position number can be found in the NAIF instrument frame kernel juno_uvs_v06.ti at the NAIF website. Thus, the effective resolution in the spin direction at mirror position 81 is $0.2/[\cos(27.06)]^2 = 0.25°$ and at position 0, 0.27°. This is the FWHM of the observed UVS emissions at the limb of Ganymede (Figures 4 and 5).

The second issue is the temporal resolution of the UVS pixel-list data set. During the UVS Ganymede observations, the time hack cadence in the pixel-list data was set to 8 ms. Pixel-list mode works by recording individual events and timehacks in a streaming list as they occur. Each event, either a photon or electron (high energy particle) detection, is reported as a detector x and y position along with a measure of the pulse height. Timehacks are interspersed in this stream of photon events and are time markers that allow the mapping of the photons at the correct time. Given Juno's 30 s spin period and the 8 ms time sampling of UVS, the UVS field of view moved by 0.1° in the spin plane for each

timehack. As a result, the 8 ms time sampling used by UVS for the Ganymede observations, the precise knowledge of where the emissions are measured in spin phase is limited to no better than ±0.1°, assuming our knowledge of the slit position is perfect. Finally, a detailed comparison of the relative pointing accuracy between the SRU and UVS has not been undertaken at this point in the mission. In fact, this is the first case where such detailed knowledge has been needed. A future deep dive into the pointing accuracies of all the instruments relative to one another would be an excellent and fruitful endeavor. However, given the uniqueness of this data set, the modeling of the particle precipitation performed within this paper, and the temporal and spatial resolution of the UVS instrument, we find that the −17 ms shift for the UVS data would provide the minimum acceptable shift in time and is more likely closer to correct than the −34 ms shift given the observed auroral emissions.

Further information on how the UVS data were analyzed for the two regions of interest is given below.

1. Emission Brightness calculation using modeled volume emission rates.

Given that the auroral curtain emissions observed were of the southern auroral oval, we assume that the emissions are spread over ≈7° of latitude (see Figures 4a and 4c from Greathouse et al. (2022)). Greathouse et al. (2022) described the emissions as optically thin so a tangent view of the auroral emissions would mean that the total emission would be the integral of the FOV through the observed extent of the auroral curtain. Given Ganymede's radius of 2631.2 km, the thickness of the auroral curtain is $2631.2 \times (7 \times \pi/180) \approx 321$ km. Utilizing the measured electron fluxes and the model atmospheres, we produced a prediction for the vertical volume emission rate for 135.6 nm oxygen emission and multiplied by the inferred auroral thickness. The results of this calculation are shown in Figure 5.

2. Calculation of polar cap emission

To calculate the polar cap emission rate within the 135.6 nm oxygen line, we calculated the mean spectrum over the area 60–180 west longitude and 30–90 north latitude. As can be seen in Figure 3 from Greathouse et al. (2022), this region is north of all auroral emissions as well as completely on the night side. There is significant radiation background (due to penetrating electrons) in this data so a subtraction of the mean emission on either side of the 135.6 nm emission line was used to remove that background from the integrated emission. The subtracted background rate was 1.15 R/nm. After background subtraction, the integrated 135.6 nm oxygen line strength was 8.5 R.

Finally, though it would be exciting to be able to use the UVS observations to constrain the vertical structure of the auroral emissions, it seems unwise to draw too heavily from the observed vertical profile given their probable unresolved nature.

3. Results: Analysis and Modeling of the Juno Observations

The extensive Juno data set provides the required information to answer two important questions:

1. Did Juno make measurements within the closed magnetic field line region of Ganymede's magnetosphere?
2. What is the nature of the Ganymede magnetosphere- Jupiter magnetosphere interaction and what are its effects on the atmosphere and surface?

3.1. Open Versus Closed Magnetic Field Lines

Although the measured plasma (JADE) and energetic particles (JEDI) show no sign of crossing into a closed magnetic field line region of Ganymede's magnetosphere, the measurement of the magnetic field as interpreted through modeling is seen to be either consistent (Duling et al., 2022) or inconsistent with the interpretation (Romanelli et al., 2022) that Juno remained on open magnetic field lines in its traversal of Ganymede's magnetosphere. Note, however, that while the MagnetoHydroDynamic (MHD, Duling et al., 2022) and hybrid modeling (Romanelli et al., 2022) efforts share a firm physical basis, the MHD modeling approach in contrast to the hybrid modeling approach provides a more convincing match to the vector magnetic field observed by Juno throughout the encounter. However, the lack of consistency of the models brings into question our confidence in tracing magnetic field lines throughout Ganymede's environment with sufficient accuracy to ascertain connectedness: (a) are field lines closed on Ganymede or (b) are they open -connected to both Ganymede and the Jovian ionosphere or (c) are both ends closed on Jupiter?

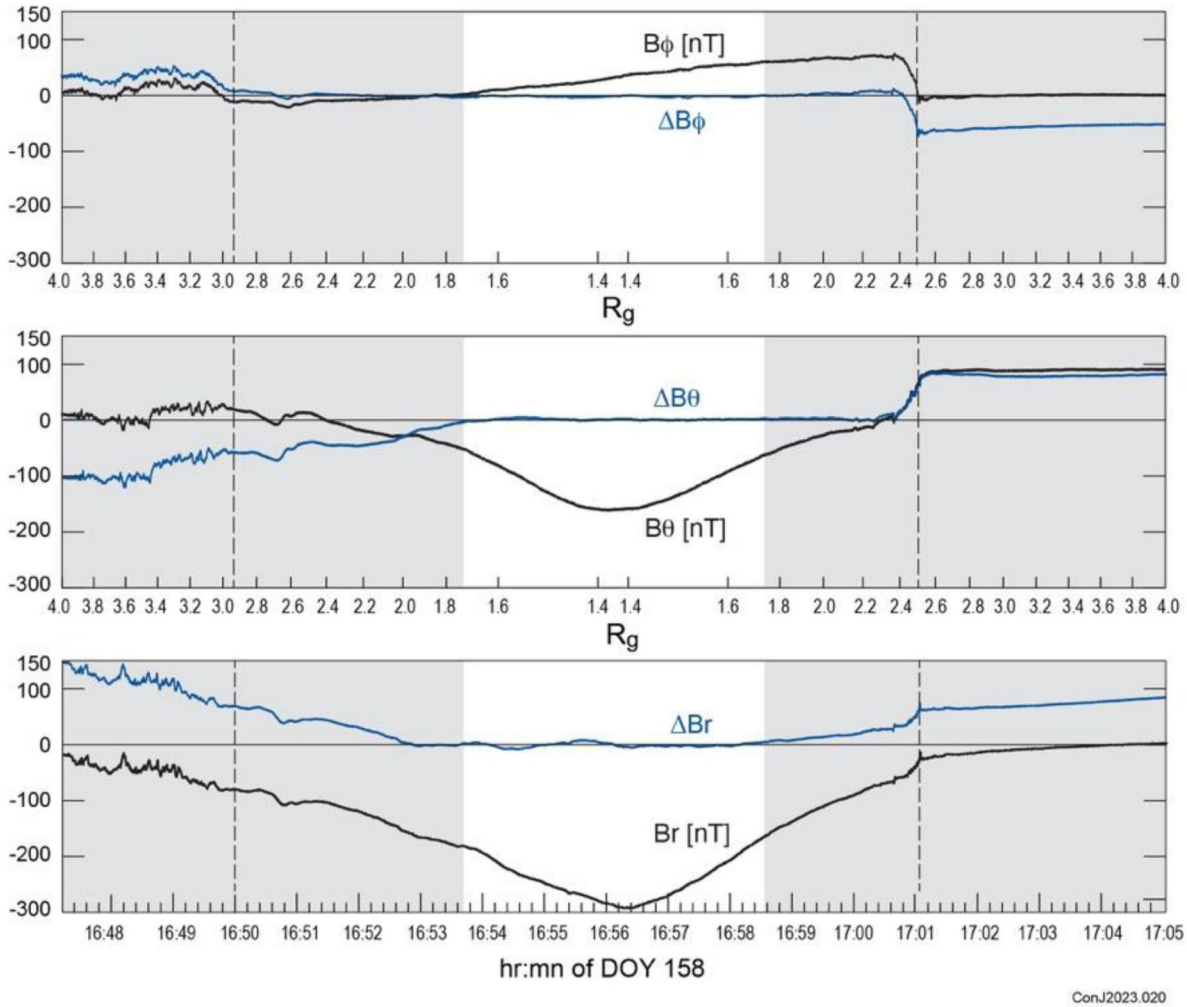

Figure 6. The magnetic field observed throughout the flyby as well as the difference (blue curve) between the model and the data is shown in the figure; RMS residuals throughout the model interval (not gray shaded) equal 2.4 nT. Field line geometry was then computed using this model, with the conclusion that no field lines were rooted in both feet on Ganymede. The units for all ordinate (y) axes are nanotesla (nT).

To address this question, a less sophisticated exercise was performed in which the field near Ganymede ($r < 1.75$ R_G) was modeled using an internal dipole and an external spherical harmonic expansion of degree 2.

3.1.1. Simplified Magnetic Dipole Interaction Model of Ganymede

The simplified modeling aims only to provide other means of extrapolating the field beyond the trajectory to trace magnetic field lines in the immediate vicinity of Ganymede. Vector observations of the field near the satellite ($R < 1.75$ R_G) were fitted with a spherical harmonic consisting of an internal dipole ($n = 1$) combined with an external quadrupole ($n = 2$). It is not intended as a model of the satellite's internal magnetic field but rather an artifice to closely fit the data with a potential field for extrapolation off the trajectory. This procedure is expected to fail where local currents contribute substantially to the field but for much of the flyby the interaction currents may be treated as "distant" currents contributing to an external field reasonably well approximated by the potential representation. The model fit during the outbound portion of the flyby provides some hope that this is the case (Figure 6). Figure 6 shows the magnetic field observed throughout the flyby as well as the difference (blue curve) between the model and the data; RMS residuals throughout the model interval (not gray shaded) equal 2.4 nT. Field line geometry was then computed using this model, with the conclusion that no field lines were rooted in both feet on Ganymede.

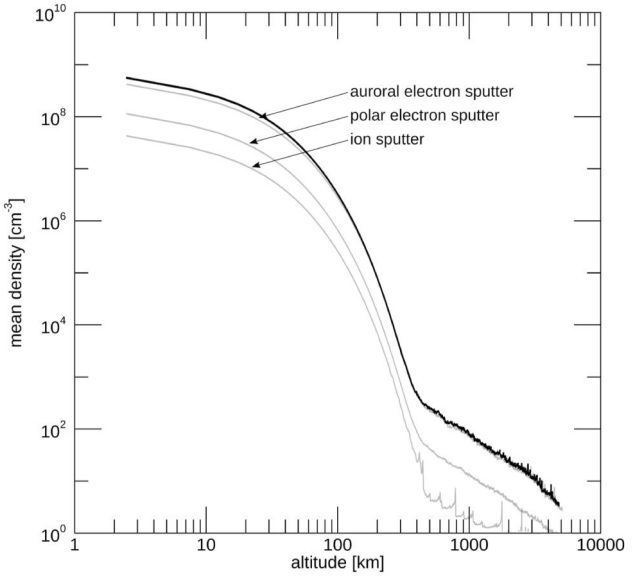

Figure 7. Sputtered O_2 density profile for three source processes: auroral electron sputtering, polar electron sputtering, and ion sputtering (all shown in gray). In addition, the overall sputtered O_2 density profile is shown in black.

This kind of analysis is only valid within a current-free volume, so its usefulness surely does not extend to the magnetopause or the wake region, but in the immediate vicinity of the satellite it can provide some guidance about field line geometry. The advantage of this approach is that the spherical harmonic expansion fits the observations well, with an RMS of 2.4 nT over the interval (closest approach 150 s), about a factor of four better fit than that provided by either of the physics-based modeling efforts. Note, however, that part of the discrepancy between the MHD model (Duling et al., 2022) and this simple model may be due to the use of the internal coefficients from the Galileo epoch. Tracing field lines from Juno's trajectory using the simplified model suggests that Juno was on field lines extending from Ganymede's northern mid-latitudes to Jupiter's ionosphere from ∼16:50 to ∼17:02, and at no time on field lines with both feet anchored on Ganymede, which is a consistent conclusion drawn from the MHD model (Duling et al., 2022). The measurements near the end of this period coincide with magnetic field signatures (amplitude of magnetic fluctuations, inbound, and field rotation, outbound) that are often used to identify the magnetopause boundary. Nevertheless, the modeling approach used here cannot be expected to perform well near such boundaries, and this method also suffers from a lack of confidence as one traces field lines beyond the immediate vicinity of the sampled region.

3.2. Magnetospheric Interaction Processes and Their Effects on the Atmosphere

3.2.1. Models Used in the Atmospheric and Ionospheric Analysis

There are four modeling tools that are used to quantify the results concerning the atmosphere and ionosphere in this paper: (a) the electron energy deposition code that produces ion production rates to be compared to the JADE ionospheric outflow and oxygen emission rates to compare with UVS based on electron input spectra from the JADE observations in the polar cap, (b) the thermal model for the atmospheric boundary layer, (c) a sputtered atmosphere model based on the work of Vorburger et al. (2022) supplemented with calculations of collisional effects in a manner similar to the work of Carberry Mogan et al. (2022) and (d) the polar cap ionospheric model used to show that the production rates of (a) are sufficient to provide the ion outflow observed by JADE. We describe each of these briefly below to clarify their design and applicability.

3.2.1.1. Electron Energy Deposition Model

The column depth of the Ganymede atmosphere is only marginally collisional according to our atmospheric modeling at altitudes below 100 km. Therefore, for simplicity, we have chosen to treat the electron transport as a downward mono directional stream model that accounts for local secondary electron production by including the secondary electron energy distributions obtained in laboratory measurements by Opal et al. (1971). The ion production rates from the major atmospheric constituents O_2 and H_2 are from Straub et al. (1996) and extrapolated to more than 1 keV using Sharma and Sharma (2019). The H_2O cross sections for electron impact were taken from Straub et al. (1998) and extrapolated in a similar fashion as described above. The electron fluxes used in our calculations are extracted from the 45° downward loss cone observations from JADE described for the polar cap in Allegrini, Bagenal, et al. (2022) and for the reconnection region described in Ebert et al. (2022). The only ultraviolet emissions that are included are those from oxygen at 135.6 and 130.4 nm for electron impact on H_2O (Makarov et al., 2004) and O_2 (Kanik et al., 2003).

3.2.1.2. Thermal Modeling of the Atmospheric Boundary Layer

All previous models have assumed that a hot Maxwellian population of electrons—presumably of ionospheric origin—are used to determine the exciting electron population that leads to the O_2 electron impact dissociative excitation of O_2 at 130.4 and 135.6 nm. Typical assumptions for this electron distribution are a 100 eV Maxwellian with an electron density of 300 per cc. We instead used the measured JADE population, albeit at high

altitudes. The Maxwellian electrons because of their energy distribution are over 20 times more effective in creating the oxygen emissions that results from the energy dependence of their cross sections. Therefore, to exclude the possibility that a "morphed" precipitating electron population is not converting to a hot thermal population near the surface where the O_2 atmospheric boundary layer is present and produces the observed emission, we constructed a simple thermal model of the electron population (Schunk & Nagy, 2000) in this boundary layer region. The energetic electron heating of the thermal electron population was modeled using the JADE energetic electrons impinging on the measured ionosphere (Buccino et al., 2022) via the methodology of Swartz et al. (1971). This heating rate is balanced by the electron ro-vibrational cooling by the primary constituents O_2 (Dalgarno, 1968; Prasad & Furman, 1974) and H_2 (Waite & Cravens, 1981). The temperature where these rates are matched determines the in situ electron temperature, which in this case is very close to the neutral thermal temperature (~150K), thereby invalidating the previous assumptions for determining the O_2 column density from HST observations, based on a hot Maxwellian electron population.

3.2.1.3. Global Sputtered Atmosphere Model

To model Ganymede's atmosphere, we included two different electron populations. The first population is the polar electrons measured by JADE that reach Ganymede's polar caps, that is, regions poleward of the open-closed field line boundary (OCFB), the surface location of which we took from Duling et al., 2022). The second population is the auroral electrons, that is, electrons that are accelerated toward Ganymede's surface into Ganymede's auroral bands (e.g., Eviatar et al., 2001). In our model, the auroral bands are described by a Gaussian distribution centered around the Open Closed Fieldline Boundary with a full width half maximum of 15°. Furthermore, for polar electrons, we used the electron differential fluxes measured by JADE in Ganymede's polar cap (Allegrini. et al., 2022a), while for auroral electrons, we used electron measurements taken by JADE in the magnetopause current layer (see Ebert et al., 2022 concerning the applicability of these electrons to Ganymede's auroral regions). To calculate the sputtered neutral particle fluxes, we used the sputter yield curves presented in Teolis et al. (2017), Galli et al. (2016, 2017) and energy distributions as presented, for example, in Johnson et al. (2009).

For ion sputtering, we use the ion precipitation fluxes already applied to Ganymede's surface in Vorburger et al. (2022). These fluxes were obtained by coupling hybrid simulations (Fatemi et al., 2016) with a test-particle model (Poppe et al., 2018) and represent the Jovian plasma environment of Ganymede as encountered by Juno as well. The ion species included are thermal H^+ and O^+ as well as energetic H^+, O^{++}, and S^{+++}. Thermal ions cover the energy range 10 eV–100 keV, whereas energetic ions cover the energy range 1 keV–10 MeV, and both distributions are divided into 17 logarithmic bins. For more information on the implemented fluxes, the reader is referred to Vorburger et al. (2022). For the ion sputter yields, we implemented well-established species- and temperature-dependent sputter yields (e.g., Cassidy et al., 2010; Famá et al., 2007; Galli et al., 2018; Shi et al., 1995). For the energy distribution of ion-sputtered neutrals, we use the same energy distribution as for electronic sputtering, that is, a thermal energy distribution but with an additional E^{-2} tail, as has been observed in laboratory ice sputtering experiments (e.g., Johnson & Liu, 1996; Johnson et al., 2002; , 2013).

Figure 7 shows the resulting O_2 density profile obtained from the collision-less 3D Monte-Carlo exosphere model already presented for Ganymede's H_2O atmosphere in Vorburger et al., 2022). In this figure, the resulting density profile for each implemented sputtering agent discussed above (polar electrons, auroral electrons, and ions) is shown separately by the gray lines. The black line shows the total O_2 density. As O_2 is a non-condensable gas, it keeps accumulating in the near-surface atmosphere until a balance between the source and the loss rates is reached. This effect is visible by the highly increased density profile at the surface and up to altitudes of a few hundred kilometers. At higher altitudes, the originally sputtered H_2 molecules dominate, which exhibit much lower but also much shallower density profiles. As one can see from this figure, auroral electron sputtering is the main source process for O_2 in Ganymede's atmosphere, resulting in O_2 density profiles approximately one order of magnitude higher than ion sputtering.

To determine a valid range of the model calculations, we experimented with combinations of the defining parameters. The factors that are not fixed (i.e., precisely determined), and for which a range of valid values can be implemented in the code are: (a) local temperature, (b) local ice concentration, and (c) FWHM of the auroral bands. The extrema of these parameters lead to the following range of O_2 column densities: Nightside polar cap—3.1 to 7.7 $\times$ 10^{15} cm^{-2} and Dayside auroral zone—1.8 to 4.5 $\times$ 10^{15} cm^{-2}.

Table 1
New O_2 and H_2 Global Production Rates Using the Measured JADE Electron Fluxes

Region	H_2 old[a] [s^{-1}]	O_2 old[a] [s^{-1}]	H_2 new[b] [s^{-1}]	O_2 new[b] [s^{-1}]
Polar cap	2.14×10^{26}	1.07×10^{26}	2.16×10^{26}	1.08×10^{26}
Auroral zone	3.33×10^{26}	1.66×10^{26}	2.13×10^{27}	1.06×10^{27}
Closed field line	4.18×10^{24}	2.09×10^{24}	6.57×10^{24}	3.28×10^{24}

Note. Figure 7 shows the vertical profiles of the emissions in columns 3 and 4. [a]Old (using electron precipitation fluxes with energies >4.5 keV as modeled in Vorburger et al., 2022). [b]New (using the electron intensities measured by Juno/JADE and discussed herein).

Table 2
Globally Averaged Column Densities With and Without JADE Electron Input

Molecule	Column density [cm^{-2}] without JADE	Column density [cm^{-2}] after JADE
H_2	2.41×10^{14}	1.09×10^{15}
O_2	4.71×10^{14}	1.77×10^{15}

3.2.1.4. Ionospheric Modeling of the Polar Cap Ion Outflows

A very simplified ionospheric model was constructed using the electron impact ionization rates for the major atmospheric species H_2, O_2, and H_2O that were calculated from the Emission Model, [3.2.1.1) above], and the photoionization cross sections where appropriate from Huebner and Mukherjee (2015). The relevant ionospheric chemistry for all production and loss processes of the modeled ions H_2^+, H_3^+, and O_2^+ in an H_2, O_2, and H_2O atmosphere were compiled from the tabulations by Moore et al. (2018) and the online database http://udfa.ajmarkwick.net/index.php. Chemical equilibrium was assumed over the atmospheric boundary layer below 100 km. Above this altitude in the region of the atmosphere that is largely non-collisional, a simple advective scheme was applied that uses a chemical equilibrium boundary condition and includes the local contributions to the ionization and chemical loss as the column of ionosphere is advected to the altitudes were JADE measured the ionosphere (Valek et al., 2022a, 2022b). A prescribed velocity profile was used and based on a profile that at the lower boundary was assumed thermal and at the upper boundary matched the JADE measured ion velocities.

3.2.2. Analysis of the Observations

Juno's Ganymede flyby data set provides a unique opportunity to study magnetospheric interaction processes and their effects on the atmosphere and surface of Ganymede. The two most noteworthy studies are: (a) the topological connection of the JADE electron energy spectrum measured in the reconnection region to the observed auroral emissions in the auroral zone and (b) the relation of ion outflow produced by polar cap electron precipitation to JADE's ion observations in the polar cap.

The extensive in situ sampling of the polar cap and the opportunity to examine reconnection taking place at the Jupiter-facing interaction boundary between Jupiter and Ganymede's magnetospheres coupled with remote sensing of the atmospheric response to particle precipitation in the ultraviolet allow detailed analysis of the process. Assumptions about the similarity of the reconnection-driven electron precipitation to that responsible for the auroral emission can be used to test our understanding of auroral processes. Furthermore, the polar cap measurements coupled with ultraviolet emissions at high latitudes poleward of the auroral zone provide simultaneous field, particle, and images that can be linked through modeling to test our present understanding of the polar ionosphere. We start our discussion with the polar cap.

The polar cap data set described earlier in the paper provides plasma, wave, and energetic particle observations that cover a broad swath over the nightside polar cap. The most noteworthy new observation is the JADE measurement of the ion outflow of H^+, H_2^+, H_3^+, and O_2^+, which we will come back to later in this discussion. In the analysis that follows, we use the measured precipitating particle spectra of the JADE plasma electron population during the PJ34 flyby. The energy flux associated with this electron population (ranging from 13 to 30,000 eV) provides 0.47–1.7 mW m^{-2} of energy flux onto the polar cap during the traversal. Correspondingly,

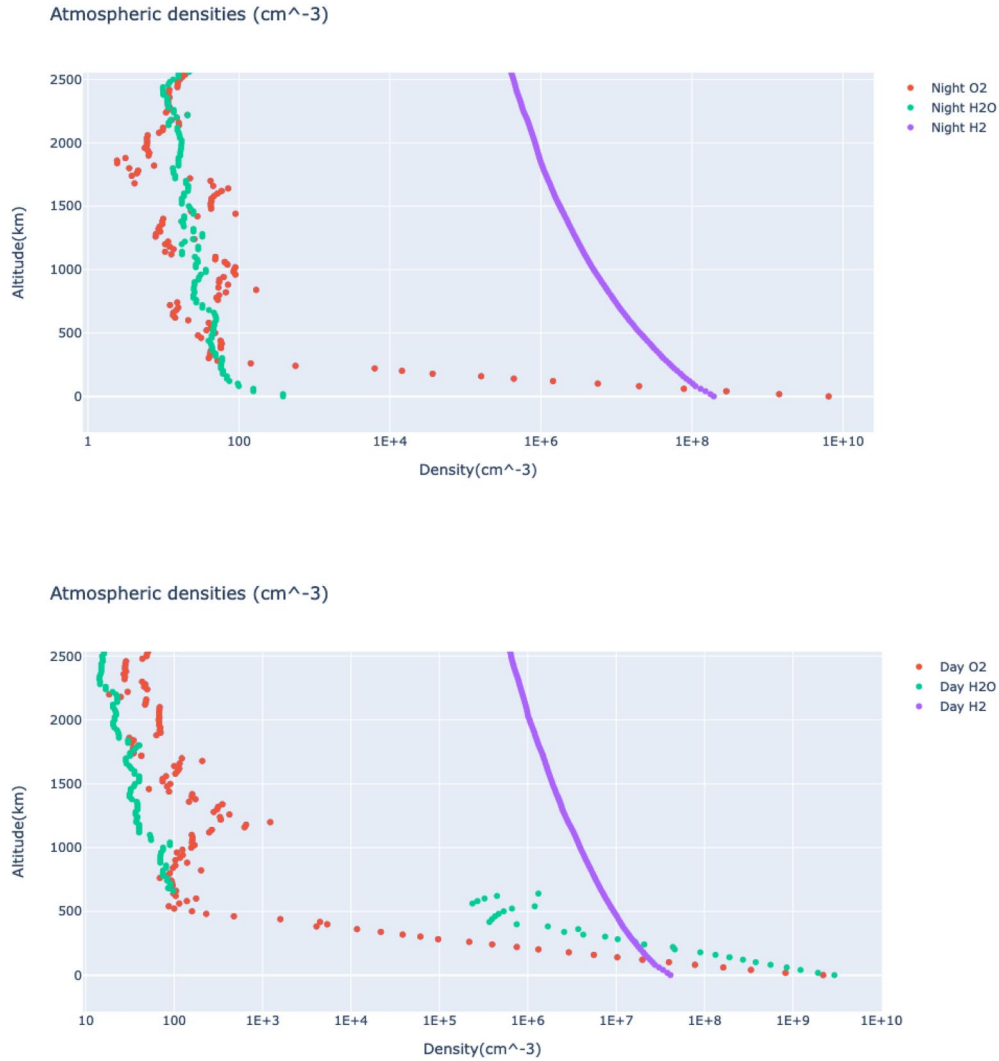

Figure 8. The neutral atmosphere model is from Vorburger et al. (2022). The model used herein is a sputtered H_2O atmospheric model with H_2 and O_2 radiolytic production added based on JADE electrons (Table 1). MIDNIGHT Column density (cm^{-2}): $H_2O = 1.04 \times 10^{10}$, $O_2 = 7.70 \times 10^{15}$, $H_2 = 4.17 \times 10^{15}$. NOON Column density ($cm^{-2}$): $H_2O = 1.41 \times 10^{16}$, $O_2 = 4.52 \times 10^{15}$, $H_2 = 1.56 \times 10^{15}$.

depending on Ganymede's position within Jupiter's plasma disk, the more energetic population measured on an earlier (day 2019-148 1700–1720 UT) orbit by JEDI and published in the Paranicas et al. (2021) paper indicate additional energy fluxes for energetic electrons above 10 keV of >100 mW m^{-2} and for energetic protons >10 mW m^{-2}.

An emission analysis tool was constructed (see Section 3.2.1 for details) to compare the simultaneous observations of the JADE electrons to the emissions measured during the flyby by UVS (see Figure 3). The low column density of Ganymede's atmosphere allows a downward discrete loss procedure to be used that takes into account secondary electron production but does not explicitly deal with primary electron degradation. These simplifying assumptions are verified upon modeling and show that less than 1% of the incident incoming electron energy is deposited in the gaseous atmosphere. The dissociative excitation cross sections for O_2 emission were taken from Kanik et al. (2003). The atmospheric structure was taken from previous atmospheric models such as Vorburger et al. (2022) and the column density was scaled to obtain the best fits to the measured OI135.6 nm intensity.

UVS observations are a key element of our comparison and are shown in Figure 3 and described in further detail in Section 2.2. Considering first the polar cap emissions observed by UVS, we averaged a large fraction of the

northern polar cap UVS observations above 30° latitude on the nightside and obtained an average OI135.6 nm emission feature of 8.5 Rayleighs. Using our analysis tool we obtain a value of 9.6 Rayleighs (15% variance) yet require an O_2 atmospheric column of 7.7×10^{15} cm^{-2} to match the observed emissions.

A similar image comparison can be obtained in the auroral belt, but in this case the UVS image can be supplemented with the vertical profile obtained of the southern aurora (see Section 2.2). The analysis again combines the emission analysis tool with the precipitating electron population observed by JADE in the reconnection region as it traversed the dayside/sub-Jovian boundary of the magnetospheric interaction region. The results are shown in Figure 5. Once more, the electron and UVS data from Juno give a very different result for the column density of O_2 that must be present in the auroral zone relative to that suggested by early models. Remarkably, whereas one might assume that there would be larger atmospheric column densities than in the polar region based on the brighter emissions, that is not the case. Rather the increased electron energy flux near the open-closed field line boundary requires a column of $\sim 4.5 \times 10^{15}$ O_2 cm^{-2} to account for the observed emissions. We note that the column densities in both the polar and auroral regions are larger than expected.

To understand the implications of the Juno results for the thickness of the O_2 atmospheric column, we also modified an existing atmospheric model to take into account the effects of the measured particle environment on the surface source rate (see Section 3.2.1). The electron data from the flyby measured by JADE between 35 eV and 30 keV were used to model the electron-induced radiolytic sources of H_2 and O_2 by including them in the earlier atmospheric model of Vorburger et al. (2022) (see Figure 5), which had so far only accounted for electrons with energies >4.5 keV. By including these lower energy electrons, a fourfold increase in the global production of H_2 and O_2 is produced. The results can be found in Tables 1 and 2 and Figures 7 and 8. This model indicates, as expected, that even though the enhanced source rate is primarily in the auroral region, the increase in the column density in the polar region is larger due to the effect of the colder surface temperatures on the O_2 lifetime. This increased O_2 and H_2 production represents an important new piece of the interaction puzzle as we will see below.

The fate of the energetic electrons and protons measured by JEDI on a previous orbit (Paranicas et al., 2021) has not been fully explored at this point and remains an open issue for future modeling. They represent a particle population that can be scattered into the closed field line region producing weak radiation belts—a phenomenon observed by comparing Juno observations to those made by the Galileo Energetic Particle Detector (Kollman et al., 2022) with a further fraction scattered onto the surface. This population is likely responsible for the extended emissions at low latitudes observed in the ultraviolet images and noted by Greathouse et al. (2022). The full impact of these two populations will require further characterization by the JUICE Particle Environment Package (Barabash et al., 2022) and/or simulation before they can be fully incorporated into models. We note that these more energetic electron populations have penetration depths of over 10^{-2} cm into the surface ice and exhibit decreasing yields of $<10^{-3}$ of sputtered and radiolytic H_2O, O_2, and H_2, which are over an order of magnitude lower than the yields at the peak of the yield curve between 100 and 1,000 eV (Teolis et al., 2017). The result is a production rate for H_2 and O_2 almost two orders of magnitude lower than the production resulting from the JADE plasma electrons (13–30,000 eV) and therefore has little effect on our previous analysis. However, most of this population will penetrate the ice and may prove to be an important source of oxidative materials in the interior of Ganymede through burial and gardening.

On the other hand, energetic protons have O_2/H_2 yields greater than the electron plasma population throughout the extended energy range from 1 to 100 keV and in ice penetration depths from 10^{-6} to 10^{-4} cm. Therefore, they represent a population that can produce O_2, H_2, and H_2O sputtering that constantly resurfaces the polar cap producing fresh ice, which is subject to adsorption of O_2 at a higher surface temperature than O_2 condensation—a process not yet incorporated into atmospheric models. However, with regard to the production of atmospheric O_2, this source is over an order of magnitude smaller than the JADE source that has already been included in our calculations.

Finally, we note that previous attempts at reconciling the aurora, for example, Eviatar et al. (2001) and Leblanc et al. (2023), created a superthermal electron near-surface plasma flux that would reproduce the emission observation based on early models of the atmosphere. In this paper, we reverse that process and use the actual Juno data to improve the estimates of the auroral emissions and then extrapolate the Juno electron data to the near surface O_2 atmosphere in order to estimate the average amount of O_2 column density that is required in both the polar and auroral regions of Ganymede. The results require the O_2 atmospheric column to be over an order of magnitude larger (4.5×10^{15} O_2 cm^{-2} vs. 2.5×10^{14} O_2 cm^{-2}) than the original value of Feldman et al. (2000).

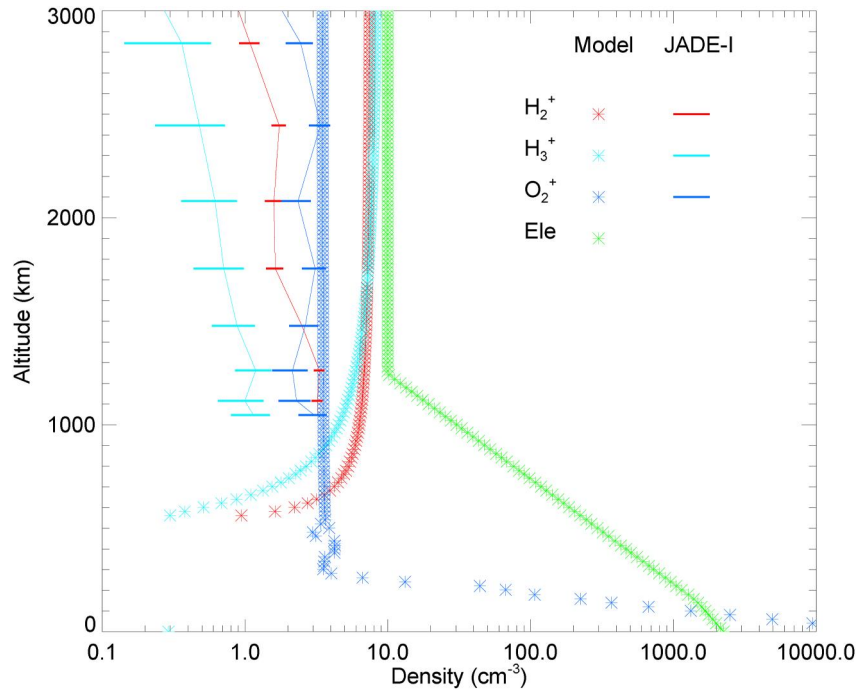

Figure 9. The modeled ionospheric profiles of H_2^+ (red), H_3^+ (magenta), and O_2^+ (blue) are compared to the acquired JADE ion outflow data (same colors, but marked with lines and error bars) in the northern polar cap. Also shown for comparison are the Juno egress (green) radio occultation profiles (Buccino et al., 2022: Dustin Buccino, 2022; Buccino, 2016). The ionospheric variance is indicated by the disagreement in the total ion density of the model when compared to the total radio - occultation electron density. Note that the JADE I ion densities have been reduced by a factor of 2.5 to match the plasma wave derived densities. The factor of 2.5 reduction represents a further uncertainty that is approximately the difference between the model and JADE-I.

We must also consider the possibility that the spatial position either at an altitude or radial distance of the Juno in situ observations does not properly characterize the exciting electron population. Potential electron modification processes such as Birkeland currents and wave particle interactions were invoked earlier in the analysis of HST observations by Eviatar et al. (2001). Eviatar et al. (2001) suggested that stochastic acceleration of electrons by electrostatic electron plasma oscillations could be a possible means of excitation of the UV emissions on Ganymede. This mechanism is unlikely, however, because the electrostatic waves observed by both Galileo and Juno in Ganymede's magnetosphere are upper hybrid waves that have an entirely different polarization than plasma oscillations. It is possible that the upper hybrid waves and related electron cyclotron waves could excite auroras since these have been discussed as possible drivers for the diffuse aurora at Earth dating back to the mid-1970s (Lyons, 1974). However, we are unaware of any studies of the efficacy of electron cyclotron waves in the production of UV emissions at Ganymede to date. There may also be relevant wave-particle interactions with whistler-mode hiss and chorus in Juno's magnetosphere (Li et al., 2022). Intense chorus and hiss were observed by Juno during its flyby of Ganymede; however, it is generally believed that the field lines sampled by Juno did not intersect the UV emission footprint (cf. Duling et al., 2022).

The acceleration of electrons by Birkeland currents, as also suggested by Eviatar et al., is observationally represented by the reconnection driven electrons observed by Ebert et al. (2022) and used in our model. However, the slowing and thermalization of electrons that might be expected in the case of a thick classical atmosphere such as Earth is minimal in the thin atmospheres of the icy moons. For example, the Maxwellian electron population required by Eviatar et al. to produce the emissions (313 cm^{-3} and 100 eV) has a factor of 20 higher efficiency for producing the OI135.6 nm emission than the JADE reconnection electron energy spectrum, but as we see below, this is not sustainable in Ganymede's boundary layer O_2 atmosphere.

Thermalization of electrons to form a hot Maxwellian can most easily be explored by producing a model in which the ionospheric electrons are heated by the incident JADE electrons and cooled by rovibrational interactions with H_2 and O_2. The measured radio occultation profiles (Buccino et al., 2022) provide constraints on the density of the

ionospheric thermal electrons that will interact with the energetic electrons to heat the boundary layer electrons. This electron heating along with the heating provided by secondary electrons from the energy degradation of the energetic primaries can quantitatively determine the role that the modified auroral electron distribution plays in enhancing the efficiency for emission in a manner similar to that first proposed by Eviatar et al. (2001). For more details on the model see Section 3.2.1.

Modeling indicates that the derived electron temperatures for all auroral atmospheric cases modeled cannot heat the ambient ionospheric electron population sufficiently to enhance the excitation of the OI135.6 nm emission. The assumed surface boundary layer temperature for the atmosphere is 150K. The only departure of the electron population from that of the ambient neutral and thermal ions occurs for the lowest column density case considered (1×10^{14} cm^{-2} O_2). Even in this extreme case the electron temperature reaches a maximum of ~2000 K due to strong rovibrational cooling by O_2 and H_2. This electron temperature is well below the 100 eV electron excitation population assumed by Eviatar et al. to bolster the efficiency for oxygen emissions for lower column density atmospheres that have been considered in the past. Furthermore, the strong effects of rovibrational cooling will also apply to more exotic electron thermalization/acceleration scenarios as well. We conclude that previous atmospheric models based on the Eviatar et al. electron excitation mechanism provide an improper constraint on the O_2 atmosphere present in the auroral zone. The use of alternative atmospheric models is advised and will be informed by the JUICE mission.

Another type of model/data comparison can be made in the polar cap. The new set of Juno measurements near Ganymede indicates energy dissipation from the system that leads to significant fluxes of outflowing ionospheric H^+, H_2^+, H_3^+, O_2^+, and water group ions. (Note that JADE actually measures 32 amu/q in the polar ionospheric outflow region, which in principle could be S^+, but this is highly unlikely based on our knowledge of the composition of Ganymede's atmosphere.) The high latitude ionospheric structure measured by JADE and its subsequent outflow have yet to be completely reconciled with the Juno radio occultation ingress (Buccino, Dustin, 2022; Buccino et al., 2022), as might be expected due to their differences in spatial location. However, using modeling that includes the JADE ion and electron plasma measurements in the polar cap, and the new Juno-inspired model atmosphere (see Figure 8), it is possible to provide a first order consistency check of our understanding of the topside polar ionosphere.

The model described in further detail in Section 3.2.1 uses a simple ion advective scheme based on the ion outflow velocities measured and inferred from JADE (Valek et al., 2022a). The lower boundary is set by chemical equilibrium below 100 km consistent with the atmospheric models used and is chosen to give the measured ratio of H_2^+ to H_3^+ ion outflow measured by JADE at 1,053 km, which is very sensitive to the altitude where photochemical equilibrium transitions to transport-dominant. Above 200 km altitude the primary atmospheric constituent becomes H_2. By constraining the ion outflow velocities using the JADE ion analysis at high altitudes in the transport dominated region of the ionospheric outflow (Valek et al., 2022a) and using the JADE precipitating electrons as the ionization source, we can match the radio occultation profile quite reasonably and simultaneously account for the measured densities of H_2^+, H_3^+, and O_2^+ in the topside ionosphere above ~1,000 km as measured by JADE at closest approach (see Figure 9). Measurement uncertainty by comparison between the JADE ion densities and the Wave electron densities is a factor of 2.

4. Summary

The Ganymede interaction is a sub-Alfvénic, subsonic interaction that is largely cylindrical in shape and stands in strong contrast to the supersonic interaction of the solar wind with planets containing magnetic fields, which have a blunt bow-shock region and a long magnetotail stretching out in the anti-solar direction.

The new set of Juno flyby measurements indicates energy dissipation and ion loss from the Ganymede system that leads to significant fluxes of outflowing ionospheric H^+, H_2^+, H_3^+, O_2^+, and water group ions, ~4×10^{26} ions per second pour out into Jupiter's magnetosphere. The amount of material leaving Ganymede is on the order of a kg per second as an ion outflow, as compared to the metric ton per second that Io produces.

The interaction also involves the transfer of a large electron energy influx (9 mW m^{-2}) from Jupiter's magnetosphere that impinges upon the surface and creates a localized boundary layer of sufficient O_2 column density to absorb a portion of this incoming energy and produce the auroral emissions observed by the Juno UVS (Figure 7). The JADE electron energy profile when utilized to determine the OI 135.6 nm emission intensity suggests a

column depth for the oxygen in the atmosphere that must be increased by a factor of ∼20 relative to the earlier pre-Juno model of Vorburger et al. (2022) that included ions in the energy range 10 eV to 10 MeV but electrons only in the energy range 4.5 keV–∼7 MeV.

The agreement of the OI135.6 nm emission using the new model atmosphere (including low energy electrons measured by JADE) for both the aurora and the polar cap provides a strong endorsement for the Juno-inspired model atmosphere. The ability to self consistently reproduce through modeling the ion outflow measured by JADE using the polar cap precipitating electron flux further strengthens the case for the new Juno-inspired atmospheric model. However, the Juno inspired atmospheric model still falls short by a factor of 2–3 in explaining the observations derived from simple emission modeling, suggesting that our understanding of the regolith interactions requires further consideration (Johnson & Jesser, 1997; Johnson et al., 2019; Trumbo et al., 2021). These complex, non-linear processes appear to be unique to the thin atmospheres of icy moons in the outer Solar System and will likely be resolved by the ESA JUICE mission (https://sci.esa.int/juice).

Data Availability Statement

The primary data sets for modeling comparison are JADE (Allegrini, Wilson, Ebert, & Loeffler, 2022), and UVS (Trantham, 2014a, 2014b). The secondary data set of relevance to the modeling are RSS (D. Buccino, 2022) and Waves (Kurth and Piker, 2022a, 2022b). Specifically, the calibrated data (Trantham, 2014a) was used and combined into the Ganymede maps (Trantham, 2014b. The Ganymede atmospheric model is from the referenced work of Vorburger et al. (2022) supplemented by the original modeling for this paper described in Section 3.2.1. The processing of the UVS data set for comparison to the model is described in Section 2.2. The electron-induced emission modeling, ionospheric modeling, and thermal modeling is written in Python specifically for this paper, is described in Section 3.2.1, and is available in Waite (2024b). The details of the data repositories that contain the information for reconstructing the figures and models can be found in the following references. Figures 2–7: Waite and Sulaiman (2024), Waite (2024a), Greathouse and Waite (2024a, 2024b), Connerney and Waite (2024), and Vorburger and Waite (2024). The python code used to produce Figure 8 and its input and output are found in Waite (2024b). JADE-I data in Figure 9 can be found in Valek et al. (2022b). The python code used to produce the model results for this figure and its input and output are found in Waite (2024b). This model also includes the fit to the ionosphere radio occultation data found in references: D. R.Buccino (2016), D. Buccino. (2022), and Buccino et al. (2022).

Acknowledgments
We thank the entire Juno Magnetospheric Working Group for the many discussions concerning the interpretation of the observations. The research presented by JHW, SB, FA, PV, RWB, GRG, TKG, and BT was funded by NASA's New Frontiers Program for Juno via a contract with the Southwest Research Institute. FB was supported at the University of Colorado as part of NASA's Juno mission supported by NASA through contract 699050X with the Southwest Research Institute. SD and JS received funding from the European Research Council (ERC) under the European Union's Horizon 2020 research and innovation programme (grant agreement No. 884711). The research (WSK) at the University of Iowa is supported by NASA through Contract 699041X with Southwest Research Institute. N.R. is supported by NASA under award number 80GSFC21M0002. S. R.C.M. was supported by Solar System Workings (SSW) Grants 80NSSC21K0152 and NNX16AR99G. The work of DB was carried out at the Jet Propulsion Laboratory, California Institute of Technology, under a contract with the National Aeronautics and Space Administration (80NM0018D0004). A.H. S. acknowledges NASA NFDAP Grant 80NSSC23K0276.

References

Allegrini, F., Bagenal, F., Ebert, R. W., Louarn, P., McComas, D. J., Szalay, J. R., et al. (2022). Plasma observations during the 7 June 2021 Ganymede flyby from the Jovian auroral distributions experiment (JADE) on Juno. *Geophysical Research Letters*, *49*(23), e2022GL098682. https://doi.org/10.1029/2022GL098682

Allegrini, F., Wilson, R. J., Ebert, R. W., & Loeffler, C. (2022). Juno J/SW Jovian Auroral Distribution Calibrated V1.0, JNO-J/SW-JAD-3-Calibrated-V1.0. *NASA Planetary Data System*. https://doi.org/10.17189/1519715

Ansher, J. A., Barnhardt, B. L., Richards, B. H., Gurnett, D. A., & Kurth, W. S. (2017). GO-J-PWS-5-DDR-PLASMA DENSITY, Galileo Jupiter pus derived plasma density full res v1.0 [Dataset]. NASA Planetary Data System. https://doi.org/10.17189/1519684

Bagenal, F., Adriani, A., Allegrini, F., Bolton, S. J., Bonfond, B., Bunce, E. J., et al. (2017). Magnetospheric science objectives of the Juno mission. *Space Science Reviews*, *213*(1–4), 219–287. https://doi.org/10.1007/s11214-014-0036-8

Barabash, S., Brandt, P., & Wurz, P. (2022). *The particle environment package (PEP) for the JUICE mission: Ready to go!*. Copernicus GmbH. https://doi.org/10.5194/epsc2022-681

Becker, H. N., Florence, M. M., Brennan, M. J., Hansen, C. J., Schenk, P. M., Ravine, M. A., et al. (2022). Surface features of Ganymede revealed in Jupiter-Shine by Juno's stellar reference unit. *Geophysical Research Letters*, *49*(23), e2022GL099139. https://doi.org/10.1029/2022GL099139

Bolton, S. J., Lunine, J., Stevenson, D., Connerney, J. E. P., Levin, S., Owen, T. C., et al. (2017). The Juno mission. *Space Science Reviews*, *213*(1–4), 5–37. https://doi.org/10.1007/s11214-0429-6

Buccino, D. (2022). Corresponding dataset for Ganymede's ionosphere observed by a dual-frequency radio occultation with Juno [Dataset]. *Zenodo*. https://doi.org/10.5281/zenodo.6206226

Buccino, D. R. (2016). Juno Jupiter gravity science raw data set V1.0, JUNO-J-RSS-1 JUGR-V1.0, NASA planetary data system (PDS). Retrieved from https://atmos.nmsu.edu/PDS/data/jnogrv_1001/

Buccino, D. R., Parisi, M., Gramigna, E., Gomez-Casajus, L., Tortora, P., Zannoni, M., et al. (2022). Ganymede's ionosphere observed by a dual-frequency radio occultation with Juno. *Geophysical Research Letters*, e2022GL098420. https://doi.org/10.1029/2022GL098420

Carnielli, G., Galand, M., Leblanc, F., Modolo, R., Beth, A., & Jia, X. (2020a). Constraining Ganymede's neutral and plasma environments through simulations of its ionosphere and Galileo observations. *Icarus*, *343*, 113691. https://doi.org/10.1016/j.icarus.2020.113691

Carnielli, G., Galand, M., Leblanc, F., Modolo, R., Beth, A., & Jia, X. (2020b). Simulations of ion sputtering at Ganymede. *Icarus*, *351*, 113918. Figures 1 and 4. https://doi.org/10.1016/j.icarus.2020.113918

Cassidy, T., Coll, P., Raulin, F., Carlson, R. W., Johnson, R. E., Loeffler, M. J., et al. (2010). Radiolysis and photolysis of icy satellite surfaces: Experiments and theory. *Space Science Reviews*, *153*(1–4), 299–315. https://doi.org/10.1007/s11214-009-9625-3

Clark, G., Kollmann, P., Mauk, B. H., Paranicas, C., Haggerty, D., Rymer, A., et al. (2022). Energetic charged particle observations during Juno's close flyby of Ganymede. *Geophysical Research Letters*, *49*(23), e2022GL098572. https://doi.org/10.1029/2022gl098572

Connerney, J. (2017). Juno J Fluxgate Magnetometer Calibrated Data V1.0 [Dataset]. *NASA Planetary Data System*. https://doi.org/10.17189/1519711

Connerney, J. E. P., Benn, M., Bjarno, J. B., Denver, T., Espley, J., Jorgensen, J. L., et al. (2017). The Juno magnetic field investigation. *Space Science Reviews*, *213*(1–4), 39–138. https://doi.org/10.1007/s11214-017-0334-z

Connerney, J. E. P., Timmins, S., Oliversen, R. J., Espley, J. R., Joergensen, J. L., Kotsiaros, S., et al. (2022). A new model of Jupiter's magnetic field at the completion of Juno's prime mission. *Journal of Geophysical Research: Planets*, *127*(2). https://doi.org/10.1029/2021JE007055

Connerney, J., & Waite, J. H. (2024). Magnetospheric-ionospheric-atmospheric implications from the Juno flyby of Ganymede figure 6. https://doi.org/10.5281/zenodo.10498166

Dalgarno, A. (1968). Collisions in the ionosphere. *Advances in Atomic and Molecular Physics*, *4*, 381.

Duling, S., Saur, J., & Wicht, J. (2014). Consistent boundary conditions at nonconducting surfaces of planetary bodies: Applications in a new Ganymede MHD model. *Journal of Geophysical Research: Space Physics*, *119*(6), 4412–4440. https://doi.org/10.1002/2013JA019554

Duling, S., Saur, J., Clark, G., Allegrini, F., Greathouse, T., Gladstone, R., et al. (2022). Ganymede MHD model: Magnetospheric context for Juno's PJ34 flyby. *Geophysical Research Letters*, *49*(24), e2022GL101688. https://doi.org/10.1029/2022GL101688

Ebert, R. W., Fuselier, S. A., Allegrini, F., Bagenal, F., Bolton, S. J., Clark, G., et al. (2022). Evidence for magnetic reconnection at Ganymede's upstream magnetopause during the PJ34 Juno flyby, 2022. *Geophysical Research Letters*, *49*, 23. https://doi.org/10.1029/2022GL099775

Eviatar, A., Strobel, D. F., Wolven, B. C., Feldman, P. D., McGrath, M. A., & Williams, D. J. (2001). Excitation of the Ganymede ultraviolet aurora. *The Astrophysical Journal*, *555*(2), 1013–1019. https://doi.org/10.1086/321510

Fama, M., Shi, J., & Baragiola, R. A. (2007). Sputtering of ice by low-energy ions. *Surface Science*, *602*(1), 156–161. https://doi.org/10.1016/j.susc.2007.10.002

Fatemi, S., Poppe, A. R., Khurana, K. K., Holmström, M., & Delory, G. T. (2016). On the formation of Ganymede's surface brightness asymmetries: Kinetic simulations of Ganymede's magnetosphere. *Geophysical Research Letters*, *43*(10), 4745–4754. https://doi.org/10.1002/2016GL068363

Feldman, P. D., McGrath, M. A., Strobel, D. F., Moos, H. W., Retherford, K. D., & Wolven, B. C. (2000). HST/STIS ultraviolet imaging of polar aurora on Ganymede. *The Astrophysical Journal*, *535*(2), 1085–1090. https://doi.org/10.1086/308889

Galli, A., Vorburger, A., Pommerol, A., Wurz, P., Jost, B., Poch, O., et al. (2016). Surface charging of thick porous water ice layers relevant for ion sputtering experiments. *Planetary and Space Science*, *126*, 63–71. https://doi.org/10.1016/j/pss201603.016

Galli, A., Vorburger, A., Wurz, P., Cerubini, R., & Tulej, M. (2018). First experimental data of sulphur ions sputtering water ice. *Icarus*, *312*, 1–6. https://doi.org/10.1016/j.icarus.2018.04.029

Galli, A., Vorburger, P., Wurz, P., & Tulej, M. (2017). Sputtering of water ice films: A re-assessment with singly and doubly charged oxygen and argon ions, molecular oxygen, and electrons. *Icarus*, *291*, 36–45. https://doi.org/10.1016/j.icarus.2017.03.018

Gladstone, G. R., Versteeg, M. H., Greathouse, T. K., Hue, V., Davis, M. W., Gérard, J., et al. (2017). Juno-UVS approach observations of Jupiter's auroras. *Geophysical Research Letters*, *44*(15), 7668–7675. https://doi.org/10.1002/2017GL073377

Greathouse, T. K., Gladstone, G. R., Davis, M. W., Slater, D. C., Versteeg, M. H., Persson, K. B., et al. (2013). Performance results from in-flight commissioning of the Juno ultraviolet spectrograph (Juno-UVS).

Greathouse, T. K., Gladstone, G. R., Molyneux, P. M., Versteeg, M. H., Hue, V., Kammer, J. A., et al. (2022). UVS observations of Ganymede's aurora during Juno orbits 34 and 35. *Geophysical Research Letters*, *49*(23), e2022GL099794. https://doi.org/10.1029/2022gl099794

Greathouse, T., & Waite, J. H. (2024a). Magnetospheric-ionospheric-atmospheric implications from the Juno flyby of Ganymede figure 4. https://doi.org/10.5281/zenodo.10498024

Greathouse, T., & Waite, J. H. (2024b). Magnetospheric-ionospheric-atmospheric implications from the Juno flyby of Ganymede figure 5. https://doi.org/10.5281/zenodo.10498124

Gurnett, D. A., Kurth, W., Roux, A., Bolton, S. J., & Kennel, C. F. (1996). Evidence for a magnetosphere at Ganymede from plasma-wave observations by the Galileo spacecraft. *Nature*, *384*, 535–537.

Hall, D. T., Feldman, P. D., McGrath, M. A., & Strobel, D. F. (1998). The far-ultraviolet oxygen airglow of Europa and Ganymede. *The Astrophysical Journal*, *499*(1), 475–481. https://doi.org/10.1086/305604

Hansen, C. J., Bolton, S., Sulaiman, A., Duling, S., Brennan, M., Connerney, J., et al. (2022). Juno's close encounter with Ganymede—An overview. *Geophysical Research Letters*, *49*(23), e2022GL099285. https://doi.org/10.1029/2022gl099285

Huebner, W., & Mukherjee, J. (2015). Photoionization and photodissociation rates in solar and blackbody radiation fields. *Planetary and Space Science*, *106*, 11–45. https://doi.org/10.1016/j.pss.2014.11.022

Jia, X., Walker, R. J., Kivelson, M. G., Khurana, K. K., & Linker, J. A. (2008). Three-dimensional MHD simulations of Ganymede's magnetosphere. *Journal of Geophysical Research*, *113*(A6), A06212. https://doi.org/10.1029/2007JA012748

Johnson, R. E., & Jesser, W. A. (1997). O_2/O_3 microatmospheres in the surface of Ganymede. *The Astrophysical Journal*, *480*(1), L79–L82. https://doi.org/10.1086/310614

Johnson, R. E., Burger, M. H., Cassidy, T. A., Leblanc, F., Marconi, M., & Smyth, W. H. (2009). In R. T. Pappalardo, W. B. McKinnon, & K. Khurana (Eds.), *Composition and detection of Europa's sputter-induced atmosphere, Europa*. University of Arizona Press.

Johnson, R. E., Carlson, R. W., Cassidy, T. A., & Fama, M. (2013). In M. S. Gudipati, & J. Castillo-Rogez (Ed.), *Sputtering of ices, the science of solar system ices* (pp. 551–581). Springer. https://doi.org/10.1007/978-1-4614-3076-6_17

Johnson, R. E., Leblanc, F., Yakshinskiy, B. V., & Madey, T. E. (2002). Energy distributions for desorption of sodium and potassium from ice: The Na/K ratio at Europa. *Icarus*, *156*(1), 136–142. https://doi.org/10.1006/icar.2001.6763

Johnson, R. E., Oza, A. V., LeBlanc, F., Schmidt, C., Nordheim, T. A., & Cassidy, T. A. (2019). The origin and fate of O_2 in Europa's ice: An atmospheric perspective. *Space Science Reviews*, *215*(1), 20. https://doi.org/10.1007/s11214-019-0582-1

Johnson, R., & Liu, M. (1996). Molecular dynamics studies of minicascades in electronically stimulated sputtering of condensed-gas solids. *Journal of Chemical Physics*, *104*(15), 6041–6051. https://doi.org/10.1063/1.471340

Kanik, I., Noren, C., Makarov, O. P., Vattipalle, P., Ajello, J. M., & Shemansky, D. E. (2003). Electron impact dissociative excitation of O2: 2. Absolute emission cross sections of the OI(130.4 nm) and OI(135.6 nm) lines. *Journal of Geophysical Research*, *108*, E11. https://doi.org/10.1029/2000JE001423

Kivelson, M. G., Khurana, K. K., Russell, C. T., Walker, R. J., Warnecke, J., Coroniti, F. V., et al. (1996). Discovery of Ganymede's magnetic field by the Galileo spacecraft. *Nature*, *384*(6609), 537–541. https://doi.org/10.1038/384537a0

Kollman, P., Clark, G., Paranicas, C., Mauk, B., Haggerty, D., Rymer, A., & Allegrini, F. (2022). Ganymede radiation cavity and radiation belts. *Geophysical Research Letters*. https://doi.org/10.1029/2022GL098474

Kurth, W. S., & Piker, C. W. (2022a). Juno e/J/S/SS Waves Calibrated Survey Full Resolution V2.0, JNO-e/J/SS-WAV-3-CDR-SRVFULL-V2.0 [Dataset]. *NASA Planetary Data System*. https://doi.org/10.17189/1522461

Kurth, W. S., & Piker, C. W. (2022b). Juno E/J/S/SS Waves Calibrated Survey Full Resolution V2.0, JNO-E/J/SS-WAV-3-CDR-SRVFULL-V2.0 [Dataset]. *NASA Planetary Data System*. https://doi.org/10.17189/1520498

Kurth, W. S., Hospodarsky, G. B., Kirchner, D. L., Mokrzycki, B. T., Averkamp, T. F., Robison, W. T., et al. (2017). The Juno waves investigation. *Space Science Reviews*, *213*(1–4), 347–392. https://doi.org/10.1007/s11214-017-0396-y

Kurth, W. S., Sulaiman, A. H., Hospodarsky, G. B., Menietti, J. D., Mauk, B. H., Clark, G., et al. (2022). Juno plasma wave observations at Ganymede. *Geophysical Research Letters*, *49*(23), e2022GL098591. https://doi.org/10.1029/2022GL098591

Leblanc, F., Oza, A. V., Leclercq, L., Schmidt, C., Cassidy, T., Modolo, R., et al. (2017). On the orbital variability of Ganymede's atmosphere. *Icarus*, *293*, 185–198. https://doi.org/10.1016/j.icarus.2017.04.25

Leblanc, F., Roth, L., Chaufray, J. Y., Modolo, R., Galand, M., Ivchenko, N., et al. (2023). Ganymede's atmosphere as constrained by HST/STIS observations. *Icarus*, *399*, 115557. https://doi.org/10.1016/j.icarus.2023.115557

Li, W., Ma, Q., Shen, X., Zhang, X., Mauk, B. H., Clark, G., et al. (2022). Driver of energetic precipitation in the vicinity of Ganymede. *Geophysical Research Letters*, *50*(6). https://doi.org/10.1029/2022GL101555

Lyons, L. R. (1974). Electron diffusion driven by magnetospheric electrostatic waves. *Journal of Geophysical Research*, *79*(4), 575–580. https://doi.org/10.1029/ja079i004p00575

Makarov, O. P., Ajello, J. M., Vattipalle, P., Kanik, I., Festou, M. C., & Bhardwaj, A. (2004). Kinetic energy distributions and line profile measurements of dissociation products of water upon electron impact. *Journal of Geophysical Research*, *109*(A9), A09303. https://doi.org/10.1029/2002JA009353

Mauk, B. H. (2022). JEDI CALIBRATED (CDR) DATA JNO J JED 3 CDR V1.0. *NASA Planetary Data System*. https://doi.org/10.17189/1519713

Mauk, B. H., Haggerty, D. K., Jaskulek, S. E., Schlemm, C. E., Brown, L. E., Cooper, S. A., et al. (2017). The Jupiter energetic particle detector instrument (JEDI) investigation for the Juno mission. *Space Science Reviews*, *213*(1–4), 289–346. https://doi.org/10.1007/s11214-013-0025-3

McComas, D. J., Alexander, N., Allegrini, F., Bagenal, F., Beebe, C., Clark, G., et al. (2017). The Jovian Auroral Distributions Experiment (JADE) on the Juno mission to Jupiter. *Space Science Reviews*, *213*(1–4), 1–97. https://doi.org/10.1007/s11214-013-9990-9

McGrath, M. A., Jia, X., Retherford, K., Feldman, P. D., Strobel, D. F., & Saur, J. (2013). Aurora on ganymede. *Journal of Geophysical Research: Space Physics*, *118*(5), 2043–2054. https://doi.org/10.1002/jgra.50122

Mogan, C., Shane, R., Johnson, R. E., Roth, L., Alday, J., Vorburger, A., et al. (2022). Callisto's atmosphere: First evidence for H2 and constraints on H2O. *Journal of Geophysical Research: Planets*, *127*(11), e2022JE007294. https://doi.org/10.1029/2022JE007294

Moore, L., Cravens, T. E., Muller-Wodarg, I., Perry, M. E., Waite, J. H., Jr., Perryman, R., et al. (2018). Models of Saturn's equatorial ionosphere based on in situ data from Cassini's Grand Finale. *Geophysical Research Letters*, *45*(18), 9398–9407. see Supplement. https://doi.org/10.1029/2018GL078162

Opal, C. B., Peterson, W. K., & Beatty, E. C. (1971). Measurements of secondary-electron spectra produced by electron-impact ionization of a number of simple gases. *The Journal of Chemical Physics*, *55*(8), 4100–4106. https://doi.org/10.1063/1.1676707

Paranicas, C., Szalay, J. R., Mauk, B. H., Clark, G., Kollmann, P., Haggerty, D. K., et al. (2021). Energetic spectra near Ganymede from Juno data. *Geophysical Research Letters*, *48*(10). https://doi.org/10.1029/2021GL093021

Poppe, A. R., Fatemi, S., & Khurana, K. K. (2018). Thermal and energetic ion dynamics in Ganymede's magnetosphere. *Journal of Geophysical Research: Space Physics*, *123*(6), 4614–4637. https://doi.org/10.1029/2018JA025312

Prasad, S. S., & Furman, D. R. (1974). Electron cooling by molecular oxygen. *Journal of Geophysical Research*, *78*(28), 6701–6707. https://doi.org/10.1029/ja078i028p06701

Romanelli, N., DiBraccio, G. A., Modolo, R., Connerney, J. E. P., Ebert, R. W., Martos, Y. M., et al. (2022). Juno magnetometer observations at Ganymede: Comparisons with a global hybrid simulation and indications of magnetopause reconnection. *Geophysical Research Letters*, *49*(23), e2022GL099545. https://doi.org/10.1029/2022GL099545

Roth, L., Ivchenko, N., Gladstone, G. R., Saur, J., Grodent, D., Bonfond, B., et al. (2021). A sublimated water atmosphere on Ganymede detected from Hubble Space Telescope observations. *Nature Astronomy*, *5*(July), 1043–1051. https://doi.org/10.1038/s41550-021-01426-9

Schunk, R. W., & Nagy, A. F. (2000). Ionospheres, Cambridge atmospheric and space science series.

Sharma, R., & Sharma, S. P. (2019). Direct and dissociative ionization cross section of oxygen molecules from threshold to 10 keV. *International Journal of Engineering and Advanced Technology*, *8*(6s3), 1365–1368. https://doi.org/10.35940/ijeat.F1241.0986S319

Shi, M., Baragiola, R. A., Grosjean, D. E., Johnson, R. E., Jurac, S., & Schou, J. (1995). Sputtering of water ice surfaces and the production of extended neutral atmospheres. *Journal of Geophysical Research*, *100*(E12), 26387–26395. https://doi.org/10.1029/95je03099

Straub, H. C., Lindsay, B. G., Smith, K. A., & Stebbings, R. F. (1998). Absolute partial cross sections for electron-impact ionization of H_2O and D_2O from threshold to 1000eV. *The Journal of Chemical Physics*, *108*(1), 109–116. https://doi.org/10.1063/1.475367

Straub, H. C., Renault, P., Lindsay, B. G., Smith, K. A., & Stebbings, R. F. (1996). Absolute partial cross sections for electron-impact ionization of H_2, N_2, and O_2 from threshold to 100eV. *Physical Review*, *54*(3).

Swartz, W. E., Nisbet, J. S., & Green, A. E. S. (1971). An analytic expression for the photoelectron-thermal electron energy transfer rate. *Journal of Geophysical Research*, *76*(34), 8425–8426. https://doi.org/10.1029/ja076i034p08425

Teolis, B. D., Plainaki, C., Cassidy, T. A., & Raut, U. (2017). Water ice radiolytic O_2, H_2 and H_2O yields for any projectile species, energy, or temperature: A model for icy astrophysical bodies. *Journal of Geophysical Research: Planets*, *122*(10), 1996–2012. https://doi.org/10.1002/2017JE005285

Trantham, B. (2014a). Juno Jupiter UVS calibrated data archive V1.0, PDS atmospheres (ATM) node. https://doi.org/10.17189/c32j-7r56

Trantham, B. (2014b). The calibrated data (Trantham, 2014a) was used and combined into the Ganymede maps. The calibrated UVS data is located at Retrieved from https://pds-atmospheres.nmsu.edu/cgi-bin/getdir.pl?dir=DATA%26volume=jnouvs_3001

Trumbo, S. K., Brown, M. E., & Adams, D. (2021). The geographic distribution of dense-phase O_2 on Ganymede. *The Planetary Science Journal*, *2*(4), 139. https://doi.org/10.3847/PSJ/ac0cee

Valek, P. W., Waite, J. H., Allegrini, F., Ebert, R. W., Bagenal, F., Bolton, S. J., et al. (2022a). In situ ion composition observations of Ganymede's outflowing ionosphere. *Geophysical Research Letters*, *49*(24), e2022GL100281. https://doi.org/10.1029/2022GL100281

Valek, P. W., Waite, J. H., Allegrini, F., Ebert, R. W., Bagenal, F., Bolton, S. J., et al. (2022b). In situ observations of Ganymede's outflowing ionosphere [Dataset]. *Geophysical Research Letters. Zenodo*. https://doi.org/10.5281/zenodo.7377687

Vorburger, A., & Waite, J. H. (2024). Magnetospheric-ionospheric-atmospheric implications from the Juno flyby of Ganymede figure 7. https://doi.org/10.5281/zenodo.10498189

Vorburger, A., Fatemi, S., Galli, A., Liuzzo, L., Andrew, R., & Wurz, P. (2022). 3D Monte-Carlo simulation of Ganymede's water exosphere. *Icarus*, *375*, 114810. https://doi.org/10.1016/j.icarus.2021.114810

Waite, J. H. (2024a). The files included in this upload contain the data and information to reproduce Figure 3 in paper 2023JE0078593 that will be published in Journal of Geophysical Research Planets. The paper is entitled Magnetospheric-Ionospheric-Atmospheric Implications from the Juno Flyby of Ganymede. https://doi.org/10.5281/zenodo.10493845

Waite, J. H. (2024b). jhwaitejr v1-alpha. https://doi.org/10.5281/zenodo.10632193

Waite, J. H., & Cravens, T. E. (1981). Vibrational and rotational cooling of electrons by molecular hydrogen. *Planetary and Space Science*, *29*(12), 1333–1338. https://doi.org/10.1016/0032-0633(81)90099-4

Waite, J. H., & Sulaiman, A. (2024). Magnetospheric-ionospheric-atmospheric implications from the. Juno flyby of Ganymede figure 2. https://doi.org/10.5281/zenodo.10493801

Weber, T., Moore, K., Connerney, J., Espley, J., DiBraccio, G., & Romanelli, N. (2022). Updated spherical harnomic magnetic field moments of Ganymede from the Juno flyby. *Geophysical Research Letters*, *49*(23). https://doi.org/10.1029/2022GL098633

Williams, D. J., Mauk, B., & McEntire, R. W. (1998). Properties of Ganymede's magnetosphere as revealed by energetic particle observations. *Journal of Geophysical Research*, *103*(A3), 17523–17534. https://doi.org/10.1029/98JA